Eurasian Journal of Physics and Functional Materials

Volume 9 | Number 3

Article 5

Pages: 1 - 1

2025

Agrogenic waste-derived biochar as green functional material for aqueous adsorption of uranium (U6+) radio-pollutant: A review

Stephen Sunday Emmanuel
Department of Industrial Chemistry, Faculty of Physical Sciences, University of Ilorin, P. M. B. 1515, Ilorin, Nigeria, stephenemmanuel6011@gmail.com

Ademidun Adeola Adesibikan
Department of Industrial Chemistry, Faculty of Physical Sciences, University of Ilorin, P. M. B. 1515, Ilorin, Nigeria

Ebenezer Temiloluwa Abimbola
Department of Medical Biotechnology, Moscow Institute of Physics and Technology (MIPT), Russia

Olumide James Oluwole
Department of Industrial Chemistry, Faculty of Physical Sciences, University of Ilorin, P. M. B. 1515, Ilorin, Nigeria

Mustapha Omenesa Idris
Department of Pure and Industrial Chemistry, Kogi State University (Prince Abubakar Audu University), P.M.B 1008, Anyigba, Kogi State, Nigeria, idrismustapha770@gmail.com

Recommended Citation

Emmanuel, Stephen Sunday; Adesibikan, Ademidun Adeola; Abimbola, Ebenezer Temiloluwa; Oluwole, Olumide James; and Idris, Mustapha Omenesa (2025) "Agrogenic waste-derived biochar as green functional material for aqueous adsorption of uranium (U6+) radio-pollutant: A review," *Eurasian Journal of Physics and Functional Materials*: Vol. 9: No. 3, Article 5.
DOI: https://doi.org/10.69912/2616-8537.1251

REVIEW

Agrogenic Waste-derived Biochar as Green Functional Material for Aqueous Adsorption of Uranium (U^{6+}) Radio-pollutant: A Review

Stephen S. Emmanuel [a,**], Ademidun A. Adesibikan [a], Ebenezer T. Abimbola [b], Olumide J. Oluwole [a], Mustapha O. Idris [c,*]

[a] Department of Industrial Chemistry, Faculty of Physical Sciences, University of Ilorin, P. M. B. 1515, Ilorin, Nigeria
[b] Department of Medical Biotechnology, Moscow Institute of Physics and Technology (MIPT), Russia
[c] Department of Pure and Industrial Chemistry, Kogi State University (Prince Abubakar Audu University), P.M.B 1008 Anyigba, Kogi State, Nigeria

Abstract

Uranium is a versatile radioactive element employed in various high-stakes applications, including nuclear power generation, nuclear weapons, radiation therapy, geological dating, nuclear submarines, and ships, etc. However, the escape of uranium to the environment has become a serious pollution and health concern, especially the pollution of water bodies. Thus, the goal of this study is to review the sequestration of uranium radio-pollutants using agrogenic waste-derived biochar (AWDBC) and empirically discuss key findings. Notably, the adsorption capacity analysis found that various AWDBC have a maximum uranium removal capacity of 4.71−1527.02 mg/g (with modified AWDBC coming to the fore) and can be reused up to 3−6 cycles with an average adsorption efficiency of 40 - >96% at the nth cycle. Moreover, it was discovered that the best-fit isotherm and kinetic modeling are the Langmuir and pseudo-second-order models, with R^2 ranging from 0.85 to 1.0. Thermodynamically, the majority of the adsorption operations are spontaneous processes associated with a disorder upsurge at the solid-liquid interface. Also, from the mechanism standpoint, chemisorption, electrostatic interactions, π-π interactions, ion exchange, and complexation through oxygen-containing functional groups govern the uranium sequestration operation. In the end, areas for future research were highlighted based on knowledge gaps identified in order to inform future researchers on possible aspects of the research to improve in the field. The findings of this study suggest that uranium in wastewater and industrial runoffs can be eco-successfully removed by green adsorption techniques utilizing agrogenic waste-derived biochar.

Keywords: Adsorption, Agro-waste biochar, Nuclear effluent, Uranium (VI), Radio-contaminant, Wastewater treatment

1. Introduction

Uranium is the 26th most abundant element in seawater and the 49th most abundant element on Earth, discovered by the German chemist Martin Heinrich Klaproth in 1789 [1−4]. Also, it is among the naturally occurring elements of the periodic table that make up the world and profoundly shape the structure and face of planet Earth by participating in the nuclear chain reaction [1,3,5,6]. Specifically, uranium is a multipurpose radioactive element utilized in various high-stakes applications (Fig. 1) such as nuclear power generation, nuclear weaponry fabrication, radiation therapy, geological dating, submarines, ships, etc [2,3,7−11]. More specifically, uranium's recent advances in power generation due to the world's craving for a more sustainable energy supply and carbon neutrality have seen its utilization increase drastically in recent decades [2,3,8,12−15]. However, uranium as a versatile radioactive element has become a blessing and a curse owing to its radiological and ecological health risk when its original or depleted form escapes

Received 20 June 2025; revised 7 July 2025; accepted 27 July 2025.
Available online 7 October 2025

* Corresponding author.
** Corresponding author.
E-mail addresses: stephenemmanuel6011@gmail.com (S.S. Emmanuel), idrismustapha710@gmail.com (M.O. Idris).

https://doi.org/10.69912/2616-8537.1251

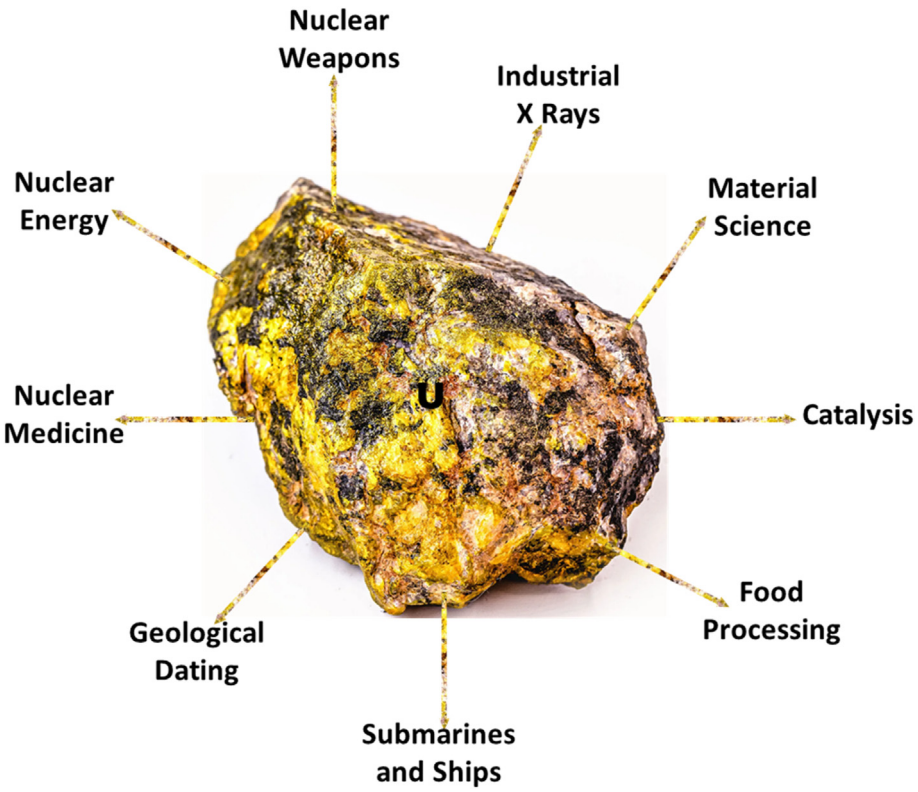

Fig. 1. Essential uses of uranium [3].

to the environment especially the aquatic environment through the discharge of spent nuclear fuel, ship accidents, phosphate fertilization activities, discharge of radio-therapy wastes from industries and hospitals, rock weathering, unguided uranium mining activities, and abundance presence in immediate war zones and nearby areas [1,2,8]. Since both natural and anthropogenic uranium pollution activities cannot be completely eradicated because it is improving the standard of living of people and contributing to societal progress, especially in energy generation, the scientific community has continued to make conscious efforts toward achieving an eco-conscious environment with low uranium radio-pollutant concentration. Notably among the available methods to combat uranium radio-pollution, adsorption using functional adsorbents like covalent/metal organic frameworks, nanomaterials, biochar, etc, has stood out [7,16–21]. Particularly, adsorption technology is eco-efficient, generates less secondary pollutants, has speedy adsorption kinetics, is easy to operate, is less expensive, and is capable of removing pollutants of interest even at very low concentrations [8,22–26]. In addition, the employment of biochar as a functional adsorbent affords the adsorption method with regenerability and scalability potential. Biochar is a carbonaceous solid residue produced through the thermochemical conversion of biomass waste like agro-waste [27–30]. Biochar has exceptional qualities, including high specific surface area (SSA), improved porosity, high biochemical/thermal stability, and enhanced active functional groups and sites that are essential for adsorption operation [31–36]. Interestingly, in recent times, when tons of agro-waste (~998 million tons yearly) are generated, more efforts have been concentrated on the use of agro-waste for biochar production [37–41]. This is because it allows tackling both water pollution and solid waste pollution concurrently.

As a research hotspot in the past years, various researchers have reviewed the utilization of the adsorption technique for the removal of uranium. For instance, in a work published in Water, the researchers reviewed and compared different biochar adsorbents that have been employed for uranium and fluoride removal [42]. Another work also reviewed different adsorbents, including Covalent organic framework, porous silica-based, biochar-based, graphene-based, amino-based, and Metal-organic framework, for the removal of uranium and thorium [43]. In a similar work, Fahad et al. reviewed graphene materials, activated carbon, and biochar for the aqueous elimination of uranium [44]. In addition, Emmanuel et al. [45] reviewed the removal of radio-contaminants in general using biochar. Thus, a comprehensive standalone

review of recent approaches to the utilization of AWDBC for uranium adsorption is necessary to empirically evaluate the effectiveness of these biochars and identify the limitations, frontiers, and future research hotspots for their development. This current work earned its novelty in the sense that it is a focused review that aims to appraise the holistic application of agrogenic waste-derived biochar (AWDBC) specifically for the sequestration of uranium from aqueous environments. The specific objectives include (1) Empirical analysis of the adsorption capacity of various AWDBCs for the removal of uranium alongside an analytical discussion of important adsorption mechanisms. (2) Holistic review of adsorption isotherm, kinetic, and thermodynamic modeling to corroborate mechanism elucidation and provide insight into process optimization. (3) Pragmatic evaluation of AWDBC reclamation, regeneration, and reusability in order to afford readers, researchers, engineers, and industries with illumination on economic values, stability, and scalability potential. (4) Underscore areas for future research work based on knowledge gaps identified in order to inform future researchers on possible aspects of the research to improve in the field. This study ultimately holds sixfold advantages in the area of circular economy advancement, SDG 7 (responsible consumption) fostering, sustainable agricultural practices, clean solid waste management, SDG 6 (water for all) promotion, and sustainable wastewater treatment.

2. Review methodology

This study made extensive use of the international comprehensive databases shown in Fig. 2, which are highly recognized for their extensive coverage of multidisciplinary literature, to compile relevant academic works until 2025. Additionally, an article search was initiated by the search terms indicated in Fig. 2, which were then utilized in various string pairings with the “OR” and “AND” operators. The review target was taken into consideration while choosing the query criteria, and only scientific publications that discussed the use of agrogenic waste-derived biochar for the sequestration of uranium radio-pollutants were selected for core analysis. Subsequently, every author went over each published article that was downloaded only by looking at the titles to expunge redundant entries. After that, any papers written in languages apart from English, as well as encyclopedias, speeches, keynotes, abstracts from seminars/conferences, as well as gray literature, were expunged. Furthermore, publishing kinds that are perceived to include non-peer-reviewed data were expunged from the research paper repository. Discrepancies were resolved by a collaborative assessment and discussion of the articles, and peer-reviewed publications that satisfied the predetermined standards were approved for the review work. In the end, 117 articles were utilized in the assembly of this work.

3. Overview of the fate of uranium in the environment and its health effects

As stated in the introductory section, it is no longer news that naturally occurring radioactive uranium is found in the Earth's crust and is possibly present in surface and groundwater because it has been accentuated to be the 26th most abundant element in seawater [1–3]. More so, it occurs naturally in rocks, soils, and minerals [1]. Moreover, uranium is lithophilic and redox-sensitive, highlighting its propensity to stick near the surface of the Earth and have a robust bond

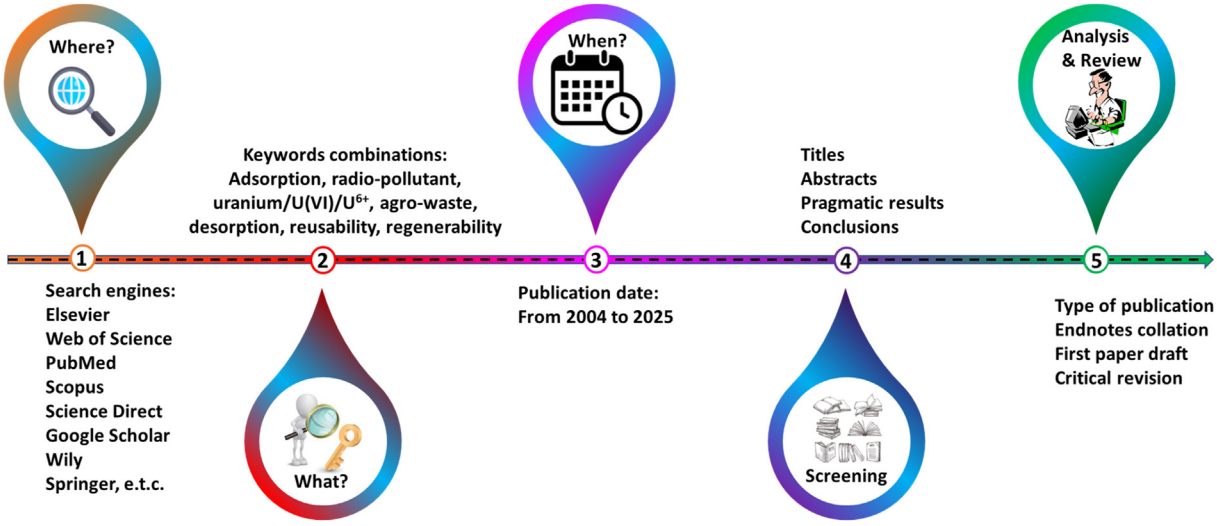

Fig. 2. Overview of review methodology. Adapted from Ref. [46].

with oxygen [1,47–50]. Furthermore, uranium can find its way into the environment through diverse anthropogenic sources, including discharged spent nuclear fuel, phosphate fertilizers, mineral exploration, radiotherapy wastes from industries and hospitals, fossil fuels combustion, mine waste, fly ash from power plants, ship accidents, and military/war use [1,8,51,52]. Natural climatic activities have the potential to transport uranium throughout the ecosystem, including the human food chain [8]. According to the literature, in contrast to intake via food products, the uranium exposure route via drinking water is recognized as a major one (accounting for about 80% according to the World Health Organization) [8,53].

In addition, uranium has a 1/2 life of around 4.5 million years and thus can remain in natural water for a long period [2,51,54,55]. Specifically, in natural waterways, the concentrations of uranium are often low; in river water, they are frequently <4 μg/L, in open saltwater, they are about 3.3 μg/L, and in groundwater, they are typically <5 μg/L. Nevertheless, higher concentrations are possible in both groundwater and surface water, with a spectrum that reaches a maximum in the mg/L range and around six orders of magnitude [1]. Additionally, uranium can dissolve into the aquifer under favorable solubility circumstances, which might contaminate sources of drinking water [8].

Notably, uranium is one of underground water's top three hazardous substances, and 70 percent of the uranium absorbed by the average human body comes from drinking water [2,56]. Human exposure to ambient uranium through the three routes shown in Fig. 3 has historically been recognized as a radiological health threat, though few epidemiological investigations have been able to reveal resultant toxicity, even in occupational settings [1,57]. However, in recent centuries, it has been accentuated that the effect of uranium on human health is more than the radiological effect. Its acute or chronic overexposure has triggered numerous health effects, including renal dysfunction, neurotoxicity, embryotoxicity, kidney damage, nephritis, fetotoxicity, lung toxicity, liver injury, and reduced bone growth [1,2,58–60,60,61]. In addition, in the oxidizing status quo, uranium present in aquatic media typically exists in the hexavalent form (U^{6+}), and the World Health Organization has identified this form of uranium as a human carcinogen [2,8]. In animal species, uranium has been shown to produce toxic impacts that can result in mortality at elevated exposure levels [1]. The possible health effect of uranium is summarized in Fig. 3.

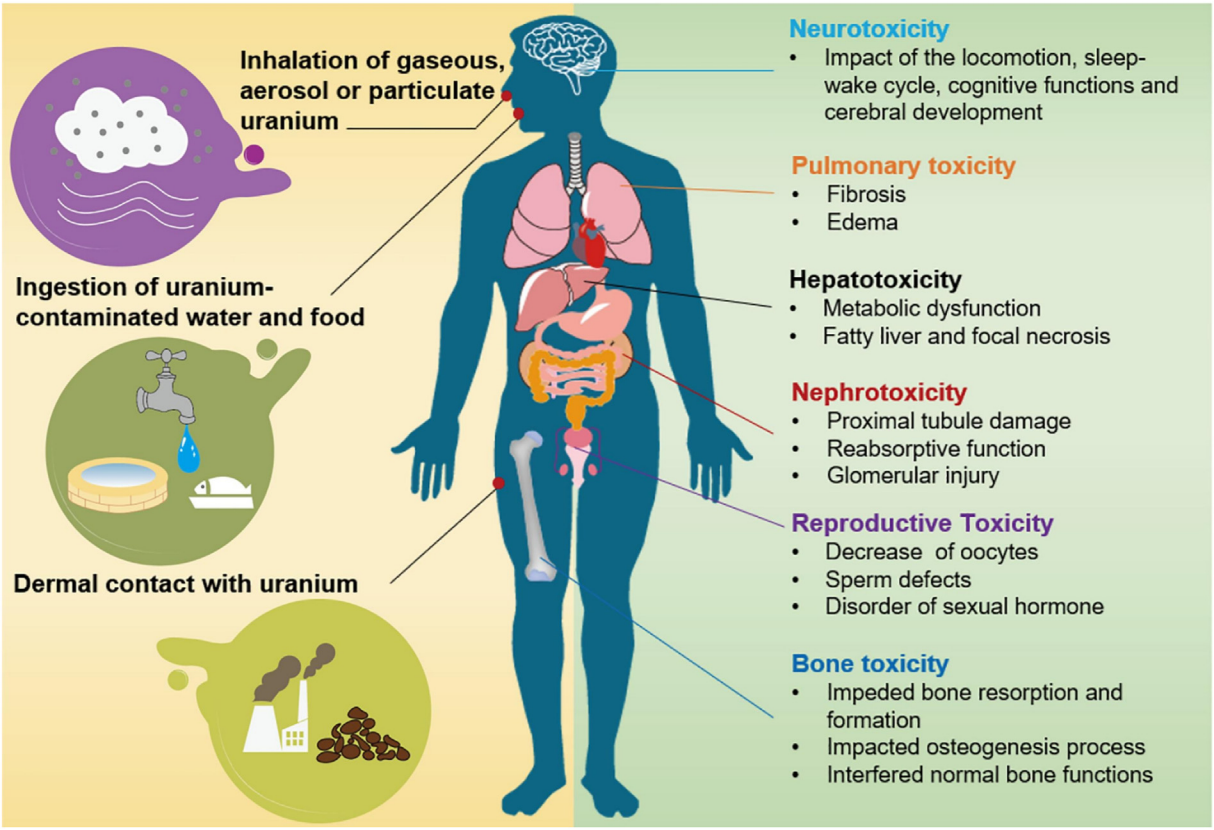

Fig. 3. The main uranium exposure routes and associated health hazards [62].

4. Adsorption performance evaluation

Adsorption performance, which is commonly stated as adsorbate mass adsorbed per gram of the adsorbent, measures the adsorbent-adsorbate affinity or the adsorbent specificity for the particular adsorbate [63,64]. The value of the adsorption capacity (q_{max}) also indicates the selectivity of the adsorbent, which is important for getting the appropriate absorption of a particular pollutant, particularly when it comes to a combination of many components [65]. Other parametric factors also influence the q_{max} value of a given biochar sorbent, and some of the variables include pollutant (uranium) initial concentration, the biochar specific surface area, pH, and contact time [26,66,67]. Consequently, in order to provide a comprehensive evaluation, the performance of the various agrogenic waste-derived biochars is generally evaluated by striking a compromise between q_{max} and SSA. The performances of various agrogenic waste-derived biochar as per q_{max}, as well as the respective AWDBC surface areas, associated sorption mechanisms, and the active functional groups, are summarized in Table 1.

For example, to remove uranium radio-pollutant from an aqueous solution, AWDBC made from cow dung and wheat straw was modified using HNO_3. It was found that the q_{max} by the oxidized wheat biochar was determined to be 355.6 mg/g at pH 4.5 and 298 K, which is a 40-fold improvement over the untreated agrogenic waste and greater than most carbon-based adsorbents, according to the authors [68]. As shown in Table 1, the q_{max} of HNO_3-oxidized cow dung biochar was also higher than that of untreated cow dung biochar, showcasing the effect of additional treatment. In addition, macroscopic investigations demonstrated that surface complexation and electrostatic interactions (ESI) governed the uranium sequestration by the AWDBC. The extremely effective adsorption of uranium was verified by FTIR investigations as being caused by the carboxyl groups on the surfaces of the AWDBC, as displayed in Fig. 4a. The R-CH_2OH groups' reducing agents promoted uranium uptake by the untreated AWDBC. Moreover, because the modified AWDBC had more negative surface charge and more surface COO functional groups than the untreated ones, they were better at sequestrating uranium. More so, the AWDBC hydrophilicity may be strengthened by the surface COO production, which would also make them more effective at eliminating uranium ions. Moreover, significant surface complexes between uranium ions and the COO groups affixed to the extremely condensed aromatic rings of AWDBC are possible [68]. Conversely, as shown in Fig. 4b for the adsorption of uranium using HNO_3 and NaOH-treated bamboo residues@polyethyleneimine biochar, imine, amide, and amine groups were observed to facilitate excellent adsorption efficiency [69].

In another uranium adsorption research, phosphorus-doped pomelo peel biochar with an excellent surface area of 1521.38 m^2/g was employed, and a remarkable adsorption capacity of 603 mg/g through complexation interaction with the biochar phosphoric acid groups was reported. EDS, FTIR, and DFT were further used to elucidate the mechanism of sequestration before and after uranium adsorption as presented in Figs. 5 and 6. Specifically, the homogeneously distributed uranium element is seen in the EDS mapping picture of the biochar following uranium sequestration, as seen in Fig. 5c. Also, the FT-IR spectra of the biochar in Fig. 5a following uranium adsorption show the emergence of a fresh peak at 914 cm^{-1}, which is linked to the O = U = O stretching vibration. Moreover, following uranium removal by biochar, there is a rise in the electron density of P-O bonds, as shown by the blue shift of the P-O stretching frequency of the FTIR. This finding indicates that P-O-H group ionization and subsequent phosphonate complexation with uranyl take place during the sequestration operation. Furthermore, according to the SEM analysis, there are no discernible changes to the fresh biochar form and structure following uranium uptake, as shown in Fig. 5d–i. As displayed in Fig. 6, the authors also did DFT calculations on several fictitious organophosphoric acid-U^{6+} complexes to shed light on the possible interaction mechanisms of phosphoric acid groups with the uranium radio-pollutant. The outcome implies that the phosphonate group has a higher propensity to form complexes with U^{6+}. On the basis of this, the potential for coordination between the phosphonate group and the uranyl ion was further examined. The ability of phosphonate to combine with uranyl to generate the stable uranyl phosphonate complex (Phosphonate-1-U) is demonstrated in Fig. 6b. Phosphate-1 and hydrated uranyl ion [$UO_2(H_2O)_5^{2+}$] have a reaction energy (ΔE) of −13,44 kcal/mol, suggesting the creation of a more stable molecule. In contrast to the hydrated uranyl ions with a U = O bond distance of 1.746 Å, the U = O bond distance in the uranyl phosphonate complex is longer, amounting to 1.782 and 1.783 Å, as shown in Fig. 6c. In addition, as shown in Fig. 6b, three complexes (phosphoric acid-1-U, phosphoric acid-2-U, and phosphoric acid-3-U) are generated when the phosphoric acid group interacts with the uranyl ion, and the +ve ΔE readings suggest that there is an energy disadvantage in the production of the uranyl-phosphoric acid combination. The aforementioned findings show that the efficient complexation of phosphonate anion with uranyl ion occurs prior to uranium adsorption on phosphorus-doped biochar. In light of this, several potential uranyl phosphonate complexes' structures were

Table 1. Summary of agrogenic waste biochar capacity (in decreasing order) and mechanism for uranium sequestration.

Agrogenic waste biochar	Surface area (m^2/g)	q_{max} (mg/g)	Method of q_{max} determination	Adsorption parameters	Mechanism	Functional groups	Ref.
Wheat straw	25.666	1527.02	Langmuir	pH = 5.0, T = 20 °C, Time = 75 min.	IEX, chemisorption, complexation, ESI, pore filling, and H-bond	Carbonyl, carboxyl, and hydroxyl groups	[79]
$KMnO_4$-modified pig manure	–	979.3	Langmuir	pH = 4.0, T = 25 °C, Time = 60 min, Dose = 10 mg, Co = 10 mg/L	Surface complexation, chemisorption, micropore filling, ESA, and IEX	NH_2, P=O and OH	[75]
Cow manure@ TiO_2@SiO_2	–	675.1	Langmuir	pH = 4.5, T = 25 °C, Time = 10 min, Co = 10 mg/L	Complexation and electrostatic interactions	Hydroxyl groups	[73]
H_2O_2-modified pig manure	–	661.7	Langmuir	pH = 4.0, T = 25 °C, Time = 60 min, Dose = 10 mg, Co = 10 mg/L	Surface complexation, chemisorption, micropore filling, ESA, and IEX		[75]
Fe_3O_4@pine needles	–	623.7	–	pH = 6.0, T = 25 °C, Time = 10 min, Dose = 100 mg, Co = 5.10^{-5} mol/L	Inner-sphere complexation	Carboxylic and hydroxyl groups	[80]
Phosphorus-doped pomelo peel	1521.38	603	–	pH = 5.0, T = 40 °C, Time = 180 min, Co = 100 mg/L	Complexation	–	[70]
Calcium phosphate modified microbial etch cotton straw	16.8	590.8	Langmuir	pH = 3.5, Dose = 5 mg, Co = 500 mg/L	Chemisorption and complexation	Phosphate group and oxygen-containing groups	[81]
Peanut shell@MnO	15.9	569.8	Langmuir	pH = 6.0, Dose = 1 mg, T = 25 °C, Co = 10 mL	ESIs, coordination reaction, precipitation, and ion exchange	OH and Mn—O	[82]
Horse manure@Bi_2O_3	–	516.5	Langmuir	pH = 4.0, T = 25 °C, Co = 10 mg/L	Surface complexation, IEX, ESA, chemisorption, precipitation, and reduction	Oxygen-containing groups	[74]
Macauba endocarp	–	417	Experiment	pH = 3.0, T = 25, Co = 5 mg/L	Chemisorption	Hydroxyls and carboxylic acids	[83]
Macaúba endocarp	–	400	Experiment	pH = 3.0, Time = 75 min, Co = 5.0 mg/L	–	–	[84]
Luffa rattan	–	382		pH = 6.0, T = 25 °C, Dose = 10 mg, Co = 225 mg/L	ESI, complexation, and physical adsorption	Carboxyl groups and hydroxyl groups	[85]
H_2O-modified pig manure	–	369.9	Langmuir	pH = 4.0, T = 25 °C, Time = 60 min, Dose = 10 mg, Co = 10 mg/L	–	–	[75]
Lotus seedpods@NH_2	20.65	367.99	Langmuir	pH = 5.0, T = 25 °C, Time = 60 min, Dose = 10 mg, Co = 100 mg/L	Complexation	Amino, carboxyl, and hydroxyl	[72]
Calcium phosphate-modified cotton straw	1.4	359.2	Langmuir	Dose = 5 mg, Co = 500 mg/L	Chemisorption and complexation	Phosphate group and oxygen-containing groups	[81]

(*continued on next page*)

Table 1. (continued)

Agrogenic waste biochar	Surface area (m^2/g)	q_{max} (mg/g)	Method of q_{max} determination	Adsorption parameters	Mechanism	Functional groups	Ref.
HNO_3-modified wheat straw	–	355.6	Langmuir	pH = 4.5, T = 25 °C, Time = 240 min, Co = 10 mg/L	Surface complexation and ESI	Carboxyl groups	[68]
Orange peel@magnesium silicate	73.9	352.6	Langmuir	pH = 4.0, T = 25 °C, Time = 120 min, Co = 25 mg/L	Inner-sphere surface complexation	C-OH, C=C, C=O, $Mg(OH)_2$ and Mg-O-Si	[76]
Durian shells	640.77	337.838	Langmuir	pH = 6.0, T = 30 °C, Time = 240 min, Dose = 5 mg, Co = 35 mg/L	Pore diffusion and ESI	OH and nitrogen-containing functional groups like C—N and C=N	[86]
Lotus seedpods	65.21	329.53	Langmuir	pH = 5.0, T = 25 °C, Time = 60 min, Dose = 10 mg, Co = 100 mg/L	Complexation	Carboxyl and hydroxyl	[72]
Watermelon rind@Fe_3O_4	86.35	323.56	Langmuir	pH = 4.0, T = 20 °C, Time = 60 min, Co = 10.0 and 200.0 mg/L	IEX, inner surface complexation, ESI, complex surface coordination, and precipitation	OH, C=C, C—H, C—O, and Fe—O	[87]
KOH-activated fish scales	1074.73	291.98	Langmuir	pH = 5.0, T = 25 °C, Time = 30 min, Co = 40 mg/L	Chemisorption and inner-sphere surface complexation	Carboxyl and amino groups	[88]
Corn straw@ ZVMn	–	274.78	Langmuir	pH = 3.0, T = 30 °C, Time = 240 min, Dose = 0.1 g/L, Co = 20 mg/L	ESI, precipitation, reduction, and complexation	Oxygen-containing groups	[89]
Peanut shell@Fe-Ni	31.4	250.78	Langmuir	pH = 5.0, T = 30 °C, Time = 240 min, Dose = 0.5 mg/g, Co = 50 mg/L	Chemical reduction, and H-bonding	C—O—C	[90]
Orange peel@MnO_2	273.25	246.3	Langmuir	pH = 5.5, T = 25.15 °C, Time = 30 min, Dose = 10 mg, Co = 50 mg/L	Inner-sphere surface complexation and chemisorption	–	[77]
HNO_3-treated rice straw	–	242.65	Langmuir	pH = 5.5, T = 25 °C, Dose = 10 mg, Co = 50 mg/L	Surface complexation, and chemisorption	–	[71]
Coconut shell@ $Ti_3C_2T_x$ and @polydopamine@ polyethyleneimine	51.6	239.7	Langmuir	Dose = 5 mg	Chemisorption, chelation, ion exchange, Electrostatic interaction, and coordination	Hydroxyl and amino groups	[78]
Bamboo residues@polyethyleneimine@NaOH	9.52	212.70	Langmuir	pH = 5.0, T = 25 °C, Co = 10.0 mg/L	Inner-sphere surface complexation, amide bonding, acetal linkage, imine bonding, and H-bonding	Imine, amide, and amine groups	[69]
Horse manure	–	186.0	Langmuir	pH = 4.0, T = 25 °C, Co = 10 mg/L			[74]
Bamboo residues@polyethyleneimine@HNO_3	10.38	185.5	Langmuir	pH = 5.0, T = 25 °C, Co = 10.0 mg/L	Inner-sphere surface complexation, amide bonding, acetal linkage, imine bonding, and H-bonding	Imine, amide, and amine groups	[69]

Orange peel	165.01	165.4	Langmuir	pH = 5.5, T = 25.15 °C, Time = 30 min, Dose = 10 mg, Co = 50 mg/L	–	–	[77]
Thermal air-treated corn cob	>400	163	Langmuir	pH = 6.0, T = 25 °C, Co = 25 mg/L	Surface complexation, ESA, and precipitation	OH, and COOH	[91]
Rice straw	–	162.54	Langmuir	pH = 5.5, T = 25 °C, Dose = 10 mg, Co = 50 mg/L	Surface complexation, and chemisorption	–	[71]
Bamboo powder@ MoS_2-PO_4	–	161.29	Langmuir	pH = 6.0, T = 25 °C, Time = 30 min, Co = 50 mg/L	Covalent bond interaction and chemisorption	P-O and C-O	[92]
Hami-melon peels	0.651	156.01	Langmuir	pH = 5.0, T = 25 °C, Dose = 0.3 g/L, Co = 30 mg/L	Chemisorption and complexation	OH and C=O groups	[93]
Orange peel	12.1	144.7	Langmuir	pH = 4.0, T = 25 °C, Time = 120 min, Co = 25 mg/L	–	–	[76]
Watermelon rind	–	135.86	Langmuir	pH = 4.0, T = 20 °C, Time = 180 min, Co = 10.0 and 200.0 mg/L	Inner surface complexation, ESI, complex surface coordination, and precipitation	OH, C=C, C—H, and C—O	[87]
Peanut shell	0.459	127.2	Langmuir	pH = 6.0, Dose = 1 mg, T = 25 °C, Co = 10 mL	ESIs, coordination reaction, and precipitation	OH	[82]
Bamboo powder@ MoS_2	–	100.14	Langmuir	pH = 5.5, T = 25 °C, Time = 60 min, Co = 50 mg/L	Covalent bond interaction and chemisorption	C-O	[92]
Camphor tree leaves	65.91	98.29	–	T = 20 °C, Co = 50 mg/L	ESA, inner-sphere surface complexation, and chemisorption	Hydroxyl, carboxyl, and amine groups	[94]
Salvadora persica branches	9.05	85.71	Langmuir	pH = 4.0, T = 25 °C, Time = 60 min, Co = 60 mg/L	IEX interaction, chemisorption, and chelation	Amino groups and the oxygen of hydroxyl and carbonyl groups	[95]
Apple tree branches@$MnFe_2O_4$	50.7	83.00	Langmuir	pH = 6.0, T = 40 °C, Time = 180 min, Dose = 1.0 g/L, Co = 10 mg/L	Complexation	Oxygen-containing groups	[96]
HNO_3-modified Cow manure	–	73.3	Langmuir	pH = 4.5, T = 25 °C, Time = 240 min, Co = 10 mg/L	Surface complexation and ESI	Carboxyl groups	[68]
Fish scales	113.34	71.59	Langmuir	pH = 5.0, T = 25 °C, Time = 30 min, Co = 40 mg/L	Chemisorption	Carboxyl	[88]
Corn cob	>400	68.82	Langmuir	pH = 6.0, T = 25 °C, Co = 25 mg/L	–	–	[91]
Cow manure	–	64	Langmuir	pH = 4.5, T = 25 °C, Time = 240 min, Co = 10 mg/L	Surface complexation and ESI	Carboxyl groups	[68]
Pine needles	–	62.7	Langmuir	pH = 6.0, T = 25 °C, Time = 50 min, Dose = 10 mg, Co = 50 μg/mL	ESI	–	[97]

(*continued on next page*)

Table 1. (continued)

Agrogenic waste biochar	Surface area (m^2/g)	q_{max} (mg/g)	Method of q_{max} determination	Adsorption parameters	Mechanism	Functional groups	Ref.
Rice husk@Fe_2O_3	109.65	53.01		pH = 4.0, T = 45 °C, Co = 60 mg/L	Inner-sphere surface complexation and chemisorption	C-C, OH, C=C, C-O, C=O, O-C=O and ferrites oxygen	[98]
Reed straw	38.945	46.35	Langmuir	pH = 5.0, T = 25 °C, Dose = 35 mg, Co = 25 mg/L	Chemisorption and complexation	O-H and C = O	[99]
Litchi shells	357.2	45.45	Langmuir	pH = 4.0, T = 25 °C, Dose = 5 mg, Co = 10 mg/L	Physisorption	–	[100]
Citrullus lanatus L. Seeds@$MnFe_2O_4$	–	27.61	Langmuir	pH = 4.0, T = 25 °C, Time = 60 min, Dose = 50 mg, Co = 30 mg/L	Surface complexation and chemisorption	Carbonyls, hydroxyls, and some carboxylic groups	[101]
Citrullus lanatus L. Seeds	–	21.24	Langmuir	pH = 4.0, T = 25 °C, Time = 60 min, Dose = 50 mg, Co = 30 mg/L	Surface complexation and chemisorption	Carbonyls, hydroxyls, and some Carboxylic groups	[101]
Wheat straw	–	8.6	Langmuir	pH = 4.5, T = 25 °C, Time = 240 min, Co = 10 mg/L	Surface complexation and ESI	Carboxyl groups	[68]
Walnut shells@Fe_3O_4	–	4.71	–	pH = 4.31, T = 35 °C, Co = 60 mg/L	Chemisorption	–	[102]

Where Co = initial concentrations of uranium (concentration of uranium before adsorption), T = Temperature.

enhanced. The five typical phosphonates may bind with uranyl ion in either a solo or synergistic coordination mode, as seen in Fig. 6c, and the coordination of phosphonate with uranyl ion is confirmed to be energetically advantageous by the -ve ΔE readings [70].

In another work, the capacity of rice straw-derived biochar to adsorb uranium from aqueous solutions was examined. Based on the findings, oxidized biochar exhibited a superior uranium uptake capacity of 242.65 mg/g compared to unoxidized biochar of 162.54 mg/g. As presented in Fig. 7, FTIR and XPS spectra of oxidized rice straw biochar were further examined prior to and following the sequestration of uranium in order to gain a better understanding of the adsorption mechanism, and the analysis confirmed that the intensity of C−O/OH functional groups reduced following uranium sequestration, signifying that the surface complexation between functional groups such as OH and COOH play a major role in the uptake of uranium by the oxidized rice straw BC [71]. Similarly, in a particular study where NH_2 functionalized lotus seedpods BC fabricated through hydrothermal technique was used for the sequestration of uranium, the maximum uptake capacity was 367.99 mg/g compared to 329.53 mg/g for the non-functionalized counterpart even though the functionalized BC has an inferior SSA (20.65 m^2/g) compared to the non-functionalized BC (65.21 m^2/g). It was accentuated that the binding of NH_2-lotus seedpods BC to U^{6+} was via complexation with amino, hydroxyl, and carboxyl groups of the AWDBC [72]. Also, the complexation sorption mechanism through the participation of OH functional groups was reported using cow manure@ TiO_2@SiO_2 biochar. However, the adsorption capacity was far more remarkable, giving 675.1 mg/g [73]. In a somewhat similar study, an adsorption capacity of 516.5 mg/g was recorded for horse manure@Bi_2O_3 biochar, and the removal mechanism was noted to be via surface complexation, ion-exchange, precipitation, chemisorption, electrostatic attraction, and reduction by oxygen-containing functional groups as shown in Fig. 8. Moreover, from the SEM analysis in Fig. 8a, it was revealed that uranium was evenly dispersed onto horse manure@Bi_2O_3 biochar, which showed that uranium ions successfully amassed onto the biochar to form new complexes [74]. A superior uranium adsorption capacity was also reported for modified pig manure biochar as presented in Table 1, with surface complexation, electrostatic attraction (ESA), chemisorption, micropore filling, and ion exchange (IEX) playing a crucial role in the adsorption operation [75].

In another study, a simple hydrothermal process was used to produce an orange peel BC and orange peel BC@magnesium silicate composite with a surface area of 12.1 m^2/g and 73.9 m^2/g, respectively, which were then

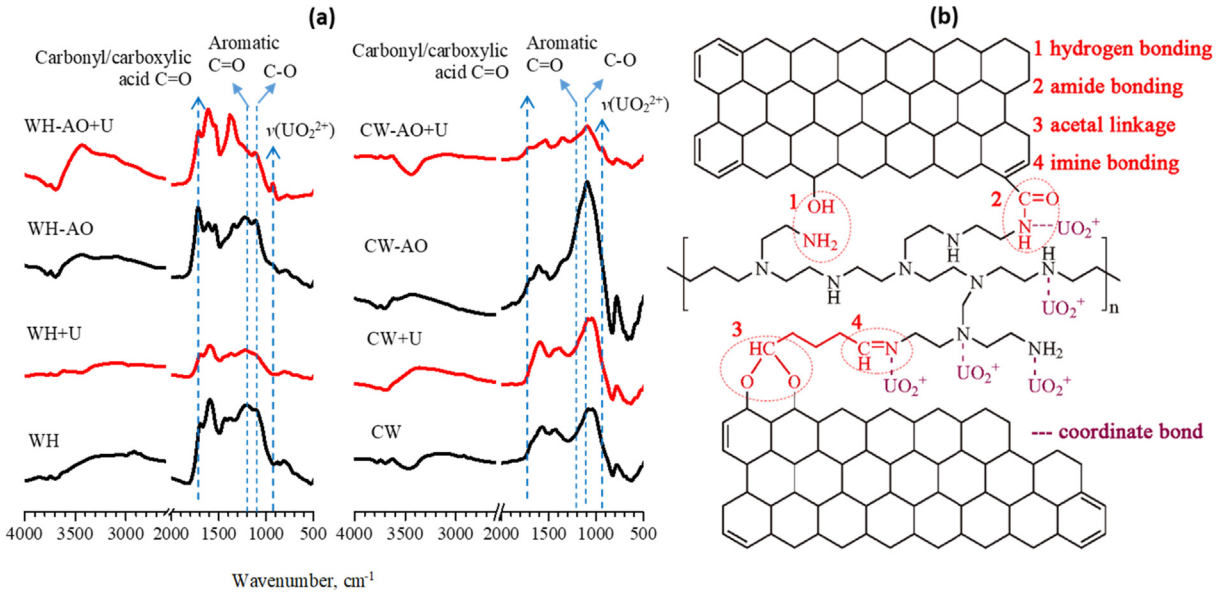

Fig. 4. (a) FTIR spectra for the unoxidized and oxidized AWDBC prior to and following uranium sequestration. "AO" designates HNO_3 oxidation [68]. (b) adsorption mechanism of HNO_3 and NaOH-treated bamboo residues@polyethyleneimine biochar for uranium uptake [69].

used to remove uranium from aqueous solution by adsorption. Notably, regardless of the presence of cations, the composite biochar was revealed to have a good sequestration capacity of 352.6 mg/g at 25 °C and pH 4 compared to bare orange peel waste biochar with 144.7 mg/g capacity under the same experimental conditions. The research finding suggested that the superior sequestration of the orange peel BC@magnesium silicate is due to inner-sphere surface complexation between uranium ions and surface functional groups (C-OH, C=C, C=O, $Mg(OH)_2$ and Mg-O-Si) of the biochar composite and this can be seen in the FTIR and XPS spectra with observable change in functional groups peaks after uranium adsorption as presented in Fig. 9a and b [76]. These findings are consistent with what was obtained for the sequestration of uranium using orange peel biochar and orange peel@MnO_2 biochar composite through inner-sphere surface complexation. Interestingly, as presented in Table 1, the sorption capacity of the biochar composite is superior to that of bare biochar (246.3 and 165.4 mg/g, respectively), and this might be due to enhanced functional groups and surface area of the biochar composite in contrast to bare biochar. [77]. A somewhat remarkable uranium adsorption capacity of 239.7 mg/g was also reported using coconut shell@ $Ti_3C_2T_x$ and@polydopamine@polyethyleneimine biochar through the participation of hydroxyl and amino groups in chemisorption, chelation, ion exchange, electrostatic interaction, and coordination mechanism. In addition, as displayed in Fig. 9c and d, the SEM analysis after uranium adsorption indicated that the surface morphology of coconut shell@ $Ti_3C_2T_x$ and@polydopamine@polyethyleneimine biochar changed and became rough [78].

5. Effect of adsorption technical operating parameters

By and large, the adsorption process is reliant on a multitude of parametric experimental factors covered in the following subsections.

5.1. Effect of pH

The pH of the solution is crucial for the adsorption operation as it can affect both the degree of ionization/oxidation of the uranium contaminant and the surface charge/functionality of the AWDBC [26,74]. Specifically, surface charge and the species distribution of AWDBC are closely associated with the environmental pH [71]. More specifically, the pH of the solution affects the uranium ion speciation and the available active adsorption sites on the AWDBC surface [95]. Also, pH governs the adsorption mechanism process since the operation involves AWDBC functional groups like OH. By and large, uranium adsorption using AWDBC has been confirmed to exhibit pH-dependent activities [74,92].

For example, the Lv et al. [72] explored the effect of pH on the adsorption of uranium using Lotus seedpods and Lotus seedpods@NH_2 derived biochar. It was reported that the two AWDBC materials largely depended on pH. Specifically, at lower pH values, it was evident that the adsorption capacities of both materials for U^{6+} were significantly low, owing to the fact that H^+ or H_3O^+ competed with UO_2^{2+} for the available adsorption sites on the AWDBC surface. Interestingly, the adsorption capacities of Lotus seedpods and Lotus

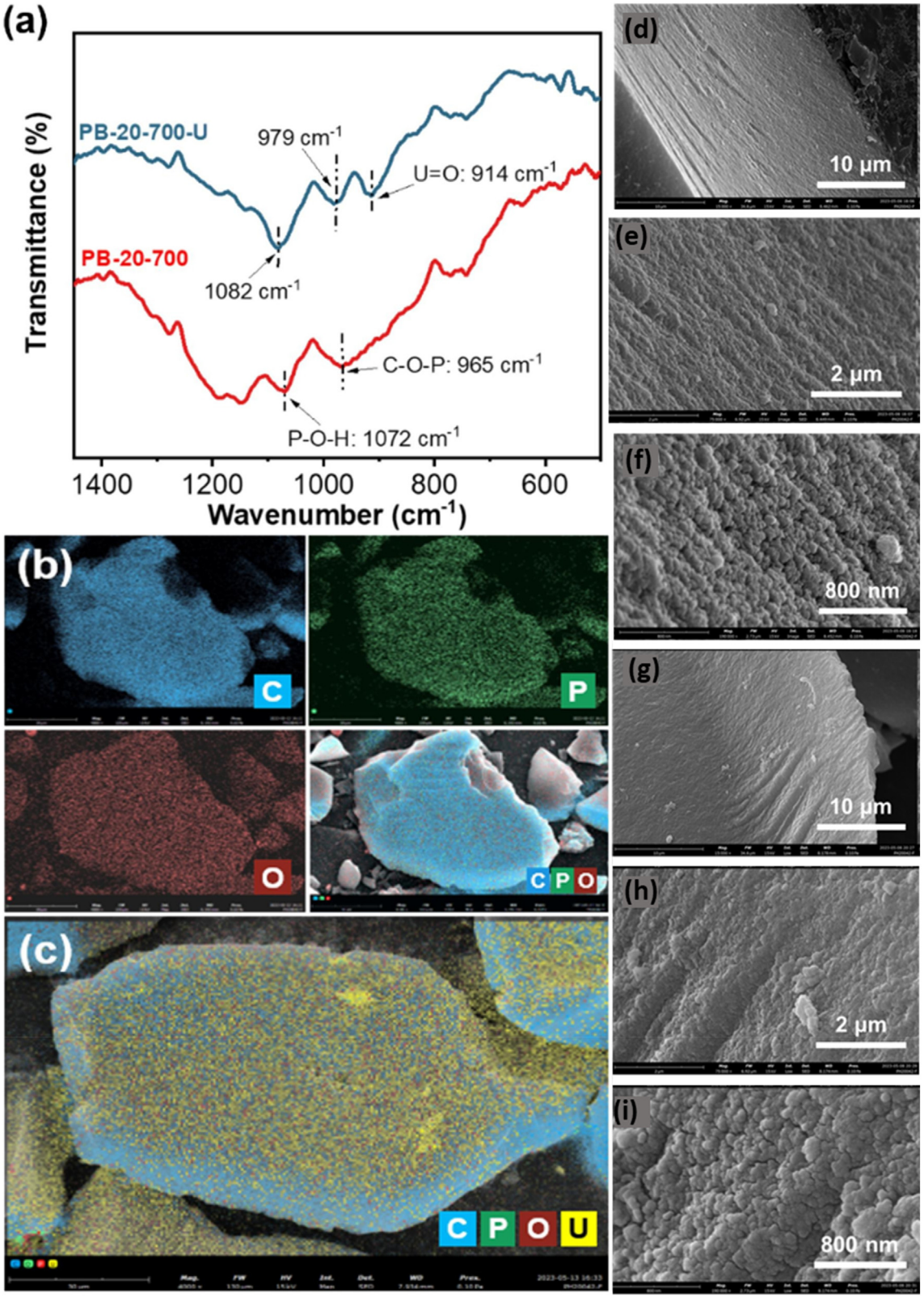

Fig. 5. FT-IR spectrum of phosphorus-doped pomelo peel BC prior to and after uranium sequestration (a). EDS mapping pictures of phosphorus-doped pomelo peel BC prior to (b) and after (c) uranium sequestration. SEM images of phosphorus-doped pomelo peel BC at diverse magnifications prior to (d–f) and following (g–i) uranium sequestration [70].

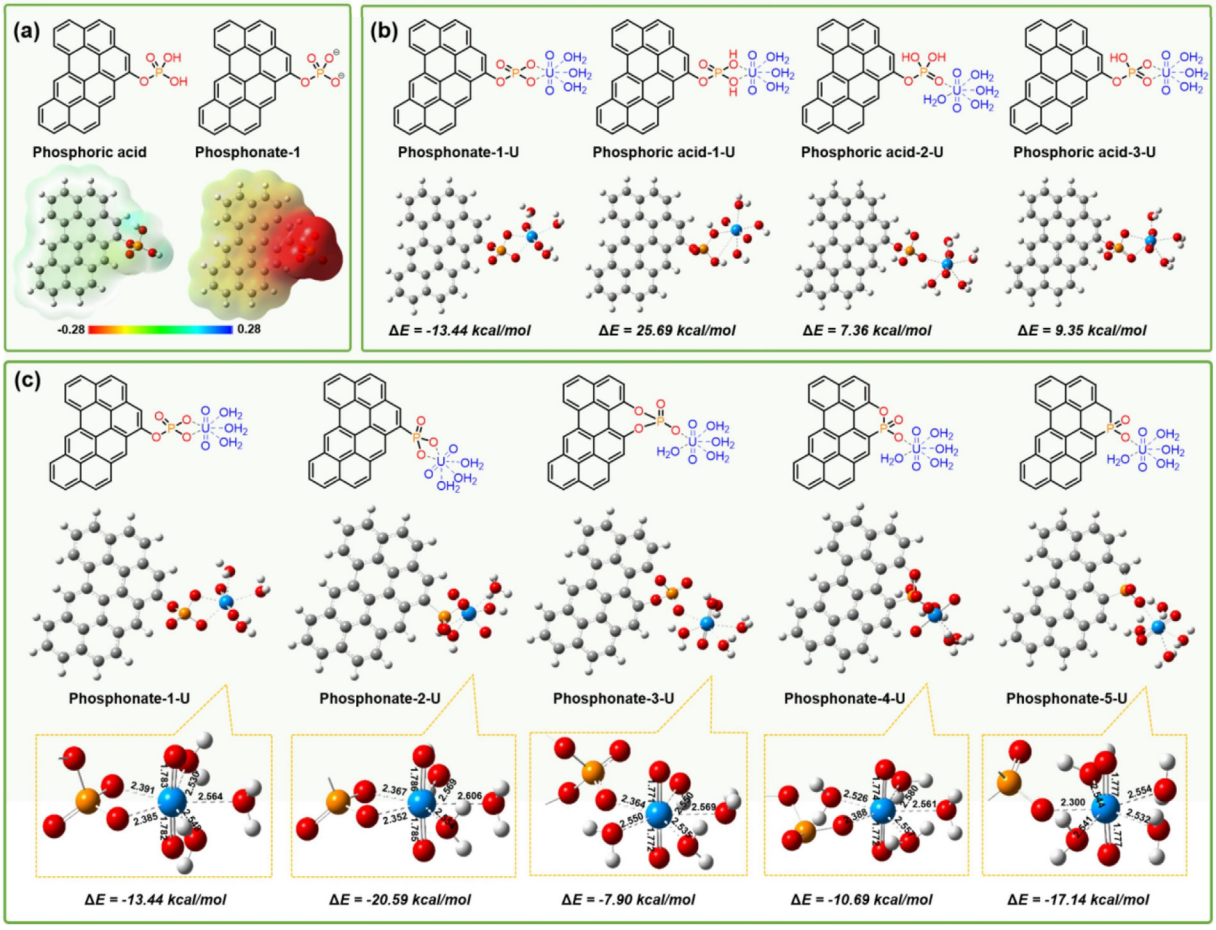

Fig. 6. Density functional theory simulation [70].

seedpods@NH_2 biochar progressively surged as the pH rose from 3 to 6 [72]. This is consistent with the explanation given for the pH dependence of U^{6+} adsorption onto reed straw biochar, with maximum removal capacity observed between pH 3 to 6 in an upward trend [99]. In a similar study, the q_e of rice straw and HNO_3-treated rice straw biochar for U^{6+} was reported to vary with pH. According to the authors, the q_e of HNO_3-treated rice straw biochar was greater than that of rice straw biochar, which improved consistently with upsurge in pH up to 5.5 but diminished subsequently [71]. This is in good agreement with the impact of pH reported for the adsorption of U^{6+} using orange peel@magnesium silicate biochar and rice husk@Fe_2O_3 biochar, where the highest q_e was observed between pH 3–6 [76,98]. Conversely, in the case of U^{6+} adsorption using modified microbial etch cotton straw biochar, the q_e only increases between pH 2 to 4, and beyond pH 4, the q_e was reported to drop gradually [81]. According to the authors, this event has a close relationship with the uranium species in solution and the surface zeta potential of the AWDBC. It was pointed out that protonation of AWDBC results in surface zeta potentials of +15.10 mV, +11.12 mV, and +8.09 mV at pH values of 1, 2, and 3, respectively [81]. An analog increasing trend was also seen for the adsorption of U^{6+} using Fe_3O_4@pine needles between pH 1–4, and this was ascribed to the presence of carboxylic moieties in the AWDBC, which demonstrate a huge affinity for the uranium cations [80].

Summarily, there is a positive correlation between q_e and pH from 2 to 6 i.e. increase in pH value from 2 to 6 results in to increase in uranium adsorption by the AWDBC and this is a testament to the fact that AWDBC can work well in harsh/acidic environment which is advantageous for nuclear wastewater remediation. Nevertheless, in our own view, extreme pH levels <2 or >8 can severely alter the surface charge of the AWDBC and the ionization/hydroxyl complexation state of the uranium ions, and negatively impact their interaction and the overall q_e.

5.2. Effect of AWDBC dose

Another crucial factor to be considered in adsorptive removal of uranium is the mass of the AWDBC

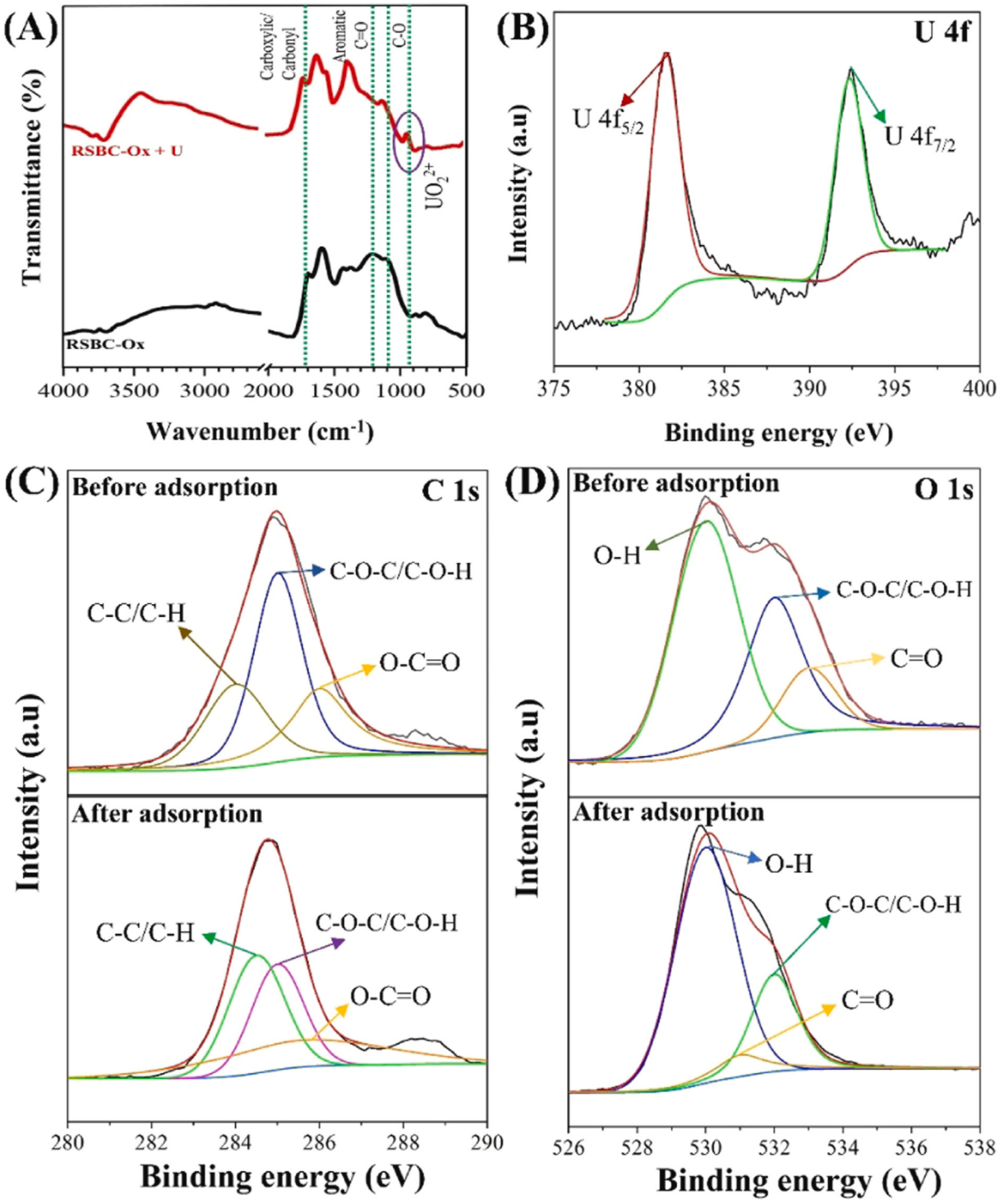

Fig. 7. (a) FTIR spectra, and (b) XPS spectra of C 1s (C) and O 1s for the oxidized rice straw biochar prior to and following uranium sequestration [71].

employed, as this dictates the numerical strength of the functional groups and active sites available for interaction [95]. For instance, in a particular research, the influence of horse manure@Bi_2O_3 biochar composite dose on the removal efficiency of uranium was explored by Liao et al. [74]. Notably, as the dosage surged from 0.1 to 0.5 g/L, the removal percentage of uranium by the AWDBC rose from 93.9 to 99.3%. It was expounded that this was because the active sites on AWDBC heightened with dosage uptick, which

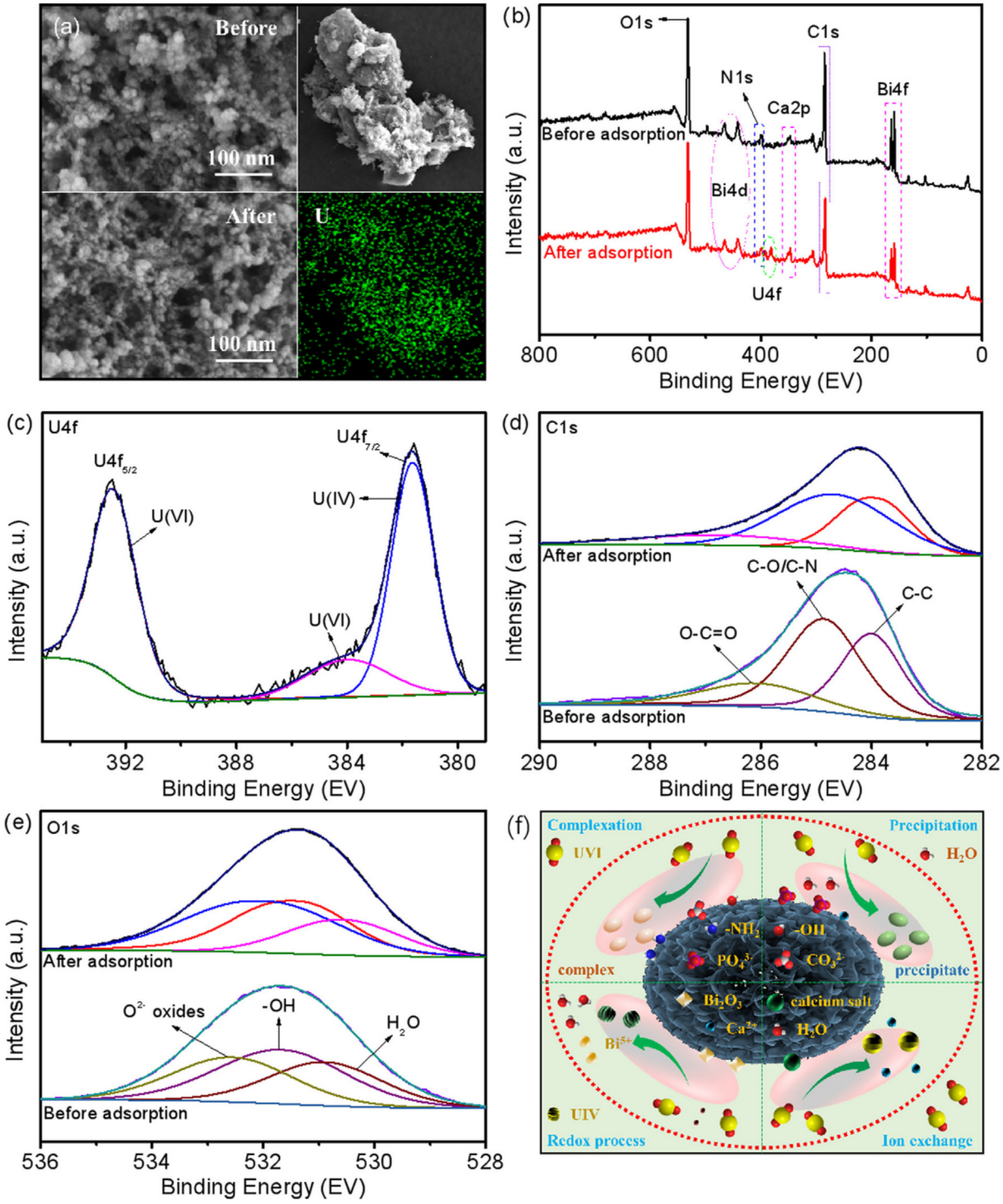

Fig. 8. (a) SEM micrographs of horse manure@Bi_2O_3 biochar prior to and following uranium sequestration, (b) Spectra of horse manure@Bi_2O_3 biochar prior to and following uranium sequestration, (c) High resolution of U4f, (d) High resolution of C1s, (e) High resolution of O1s and (f) Adsorption mechanism [74].

encouraged the formation of complexes between active sites of the horse manure@Bi_2O_3 biochar composite and uranium species. In addition, as the Bi_2O_3 dose rose, the distribution coefficient (K_d) of the biochar composite first declined gradually before rising noticeably. While the upsurge in K_d suggested that many active sites were obscured by the increasing AWDBC dose, the drop in K_d was attributed to the system's active sites becoming more exposed [74]. On the contrary, in a similar study [101], for the

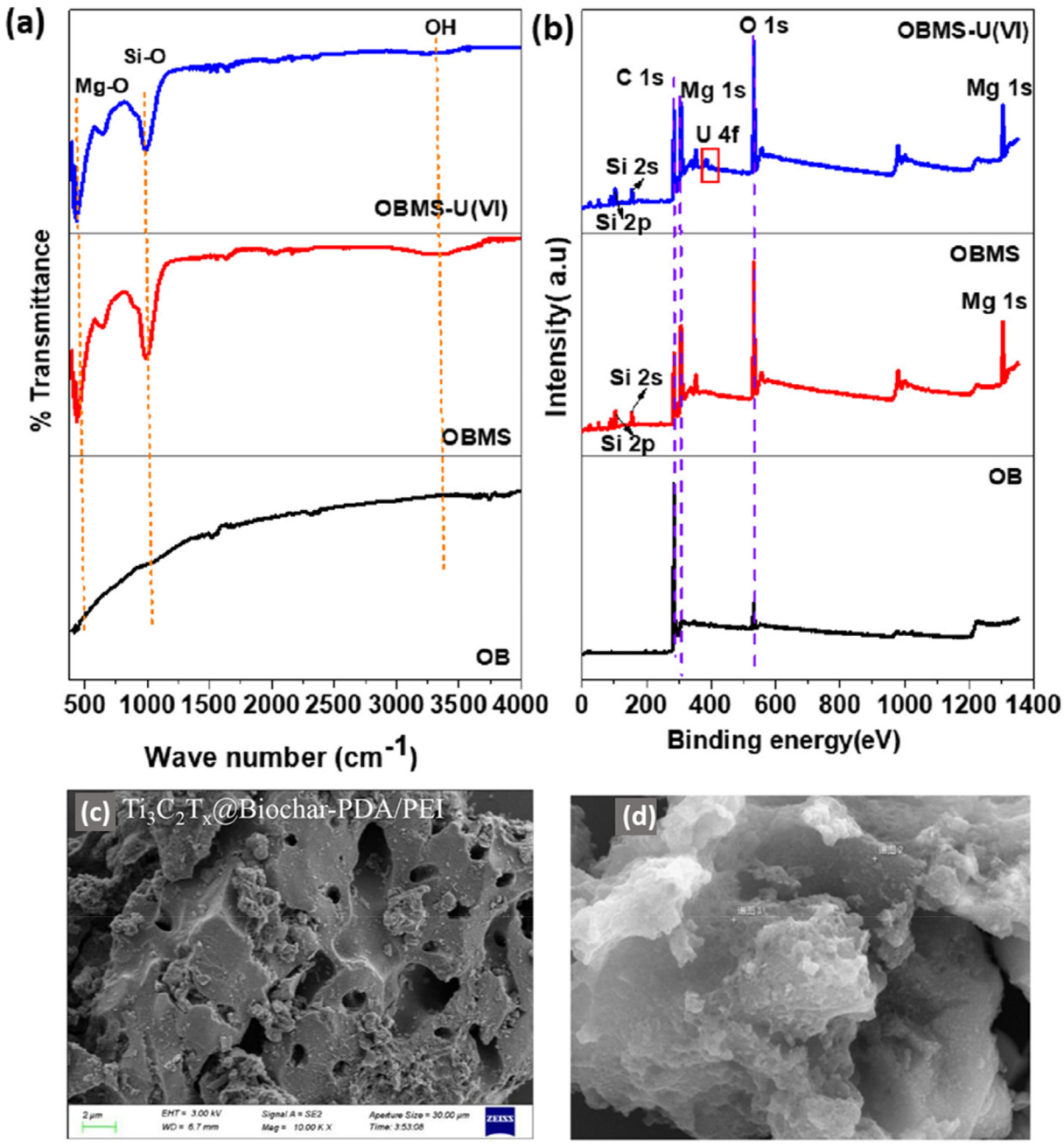

Fig. 9. (a) FT-IR and (b) XPS of orange peel biochar, orange peel@magnesium silicate biochar, and orange peel@magnesium silicate biochar after uranium adsorption [76]. SEM image of coconut shell@ $Ti_3C_2T_x$ and@polydopamine@ polyethyleneimine biochar (c) before and (d) after uranium adsorption [78].

adsorption of U^{6+} by *Citrullus lanatus* L. seeds and *Citrullus lanatus* L. seeds@$MnFe_2O_4$ biochar, the q_e was reported to diminish with an upsurge in AWDBC dosage [101].

Also, Lv et al. [72], studied U^{6+} adsorption at different AWDBC adsorbent doses. Evidently, the adsorption capabilities of U^{6+} by Lotus seedpods and Lotus seedpods@NH_2 biochar progressively declined as the dose of the adsorbent increased. This occurred because, despite a progressive rise in the AWDBC dose, the amount of uranyl ions remained constant, resulting in insufficient U^{6+} for the adsorbent to attain saturation. As a result, the U^{6+} q_e declined. The removal rate, however, showed the opposite pattern. After reaching 60%, it was found that the Lotus seedpods biochar removal rate tended to balance, and at 99.3%, the Lotus seedpods@NH_2 biochar removal rate was attained. An average AWDBC dose of 10 mg was prescribed by the

authors [72]. A similar trend was also observed in another study on the effect of reed straw biochar dose for U^{6+} adsorption. However, 35 mg was presented as the ideal dose [99].

Conclusively, as we can see, there is a positive correlation between dose and adsorption rate, but not the q_e. This is because when the AWDBC dose is increased, more active sites for adsorption/interaction are created, which speeds up the uranium adsorption process [95]. However, an excessively high AWDBC dose has negative impacts on the q_e owing to the possibility of agglomeration, which reduces the effective surface area and in turn reduces the adsorption output or because as the AWDBC dose increases, the amount of uranyl ions remains the same, leading to insufficient U^{6+} for the AWDBC to reach saturation. Interestingly, the fact that the optimal AWDBC dose for the adsorption of U^{6+} is less than 100 mg in most cases showcases the economic benefits.

5.3. Effect of initial uranium concentration

According to studies, the initial concentration of pollutants plays a crucial role in the adsorption operation [87]. By and large, at the earlier stages of adsorption operation, an increase in the initial concentration of uranium can be beneficial as it affords a greater mass transfer driving force for the uranium ions [92]. For instance, the impact of initial U^{6+} concentration on the q_e of Bamboo powder@ MoS_2 and Bamboo powder@ MoS_2-PO_4 biochar was explored by Sun's research group [92]. From the result, it was noted that the q_e of both AWDBC materials surged with an upsurge in U^{6+} initial concentration and maintained equilibrium when the maximum q_e was attained. It was expounded that this is because, as the interaction between AWDBC and the uranium surges, the driving force of the solution mass on the AWDBC surface also improves [92].

In another research, the adsorption study was carried out at different initial U^{6+} concentrations (10–100 mg/L) using watermelon rind@Fe_3O_4 biochar, and it was found that the U^{6+} q_e improved with an upsurge in uranium concentration [87]. Similarly, in another experiment, it was reported that the adsorption capacities of Lotus seedpods and Lotus seedpods@NH_2 derived biochar for U^{6+} surged as the initial U^{6+} concentration surged [72]. This is consistent with another report where it was found that upon enhancing the initial concentration of U^{6+}, the q_e of reed straw biochar also surged progressively until equilibrium was attained [99].

Summarily, there is a somewhat positive correlation between AWDBC adsorption efficiency and initial uranium ion concentration. In that, an increase in initial concentrations of uranium ions normally increases adsorption output. However, once equilibrium is reached, adsorption at this point is usually negligible, and beyond equilibrium, higher uranium concentrations can diminish the adsorption output due to the oversaturation of the employed AWDBC, and repulsion builds up between the adsorbed and available uranium ions in the reaction mixture.

5.4. Effect of temperature

The temperature has crucial importance in the adsorption operation [71]. On a general note, temperature influences the mobility of pollutant ions and the AWDBC-pollutant interface [103,104]. In addition, the temperature can also influence the viscosity of the pollutant solution and the surface charge of the AWDBC during the adsorption process.

For instance, the effect of temperature was evaluated by carrying out adsorption operations at 15.15, 20.15, 25.15, 30.15, and 40.15 °C for the removal of U^{6+} using orange peel and orange peel@MnO_2 biochar. It was demonstrated that the adsorption significantly improves with an increase in reaction temperature [77]. This is in good agreement with what was observed for the adsorption of U^{6+} using *Citrullus lanatus* L. seeds@$MnFe_2O_4$ biochar, with 45 °C giving the highest q_e, while 25 °C gave the lowest [101]. In another research, the adsorption of U^{6+} onto rice straw and HNO_3-treated rice straw biochar was carried out at five (5) different temperatures (15, 20, 25, 30, and 40 °C). It was observed that both adsorbents exhibited an upward trend in U^{6+} q_e with an uptick in temperature up to 40 °C [71]. This is in good agreement with another temperature effect study that recorded that an upsurge in temperature brought about an upsurge in U^{6+} q_e by Reed straw biochar, indicating that high temperature was advantageous for uranium removal [99].

Also, for the removal of U^{6+} using Bamboo powder@ MoS_2 and Bamboo powder@ MoS_2-PO_4 biochar, it was noticed that the upsurge in temperature enhanced the adsorption operation [92]. This is in agreement with what was observed for the removal of U^{6+} using Lotus seedpods and Lotus seedpods@NH_2 biochar. The two AWDBC adsorbents' adsorption capabilities progressively improved with an upsurge in temperature, suggesting that materials were better at adsorbing U^{6+} even at higher temperatures [72]. In a similar report, the findings revealed an evident increase in the potential q_e of calcium phosphate modified microbial etch cotton straw biochar for U^{6+} with an upsurge in adsorption temperature from 20 to 40 °C [81]. From a kinetic point of view, the uranium adsorption process is enhanced by the upsurge in reaction temperature even beyond ambient conditions, and this suggests that the

AWDBC can be employed effectively in nuclear wastewater cleanup.

5.5. Effect of contact time

The residence time greatly impacts biochar adsorption operation and chemical reactions in general [104,105]. Most adsorption operations are completed at extended residence time until equilibrium is established and no discernible change occurs [26]. Additionally, residence time affects the adsorption kinetics, which is necessary for scalability and mechanism study, indicating that it's a crucial component of the uranium adsorption operation [72].

For example, the effect of residence time on the uptake of U^{6+} by rice straw and HNO_3-treated rice straw biochar was investigated by Ahmed and co-workers. It was recorded that early in 30 min of adsorption reaction, rice straw biochar showed a quick equilibrium phase before achieving equilibrium, while HNO_3-treated rice straw biochar showed a slower process. The increased U^{6+} concentration gradient and the availability of enough active sites were attributed to the swift growth phases [71]. Also, for the adsorption of U^{6+} using Bamboo powder@MoS_2 and Bamboo powder@MoS_2-PO_4 biochar, it was observed that q_e surged significantly within 30 min for the latter AWDBC and then surged slowly afterward; while the q_e for the former AWDBC increased strongly within 60 min, and subsequently slowed down [92]. This is consistent with another report for the adsorption of U^{6+} using orange peel and orange peel@MnO_2 biochar [77]. Here, it was observed that q_e strongly surged in the earlier 30 min, afterward attained equilibrium for orange peel biochar and moved up gradually for orange peel@MnO_2 biochar. It was opined that the quick growth phases were ascribed to a large amount of unoccupied active sites on the AWDBC and a high uranium concentration gradient [77]. This is in agreement with what was accentuated by Albayari et al., where the *Salvadora persica* biochar removal capacity for uranium surged swiftly in the first 60 min until equilibrium was attained in 120 min [95].

Summarily, there is a positive correlation between AWDBC adsorption efficiency and residence time, in that the longer the contact time, the higher the adsorption efficiency until the uranium contaminant is completely removed or the active site of the AWDBC is exhausted. Nevertheless, the residence time required to reach equilibrium in uranium adsorption is contingent on the uranium initial concentration, solution pH and temperature, nature of the AWDBC, and the dose, and it varies across the board. Additionally, the decrease in q_e at a point after some time can be ascribed to the fact that in the beginning, the AWDBC has abundant unoccupied active sites for adsorption; however, with an uptick in residence time, the active sites become saturated with uranium and the adsorption operation get retarded until the maximum q_e of the AWDBC is reached, beyond which no appreciable U^{6+} adsorption takes place [26].

5.6. Effect of competing ions/co-existing pollutants

Considering the complexity of actual radioactive/nuclear wastewater, competitive/selective adsorption study, which deals with the effect of co-existing ions/pollutants, is another significant aspect of uranium adsorption that is worthy of exploration [81]. For example, the q_e of Lotus seedpods and Lotus seedpods@NH_2 biochar for U^{6+} was studied in the presence of different competing ions like Ca, K, Mg, Zn, Sr, Cs, Sm, Eu, Gd, and La. Notably, the selectivity of Lotus seedpods@NH_2 to U^{6+} was as high as 70.02% upon modification, whereas the selectivity of Lotus seedpods biochar to U^{6+} was clearly only 44.17%. It showed that following NH_2 functionalization, U^{6+} adsorption ability by Lotus seedpods biochar was markedly improved. Additionally, in contrast to other ions, Lotus seedpods@NH_2 biochar had a clear edge in the adsorption of uranium and had higher selectivity, as evidenced in the high K_d value of 8146.5 mL/g compared to Lotus seedpods biochar with a low K_d value of <1000 mL/g [72].

Also, research has shown that the humic acid surface contains copious reactive functional groups like alcohol/phenolic OH, quinone/ketone carbonyl, and carboxyl, which considerably influence the adsorption, redox, and complexation of uranium [98]. In a particular study, the impact of humic acid on uranium removal by rice husk@Fe_2O_3 biochar at pH 2.0 to 11.0 was investigated. Notably, uranium uptake by the AWDBC was marginally impacted by humic acid (1−100 mg/L) at pH less than 4, whereas at pH greater than 6.0, uranium uptake dramatically surged with an upsurge in humic acid (HA). It was suggested that this is because the negatively charged humic acid could be readily adsorbed on the +vely charged surface of the rice husk@Fe_2O_3 biochar at low pH. Then, the +vely charged AWDBC surfaces will be somewhat neutralized by this adsorption, which will aid in the sorption of +vely charged uranium species. Nevertheless, when the pH is > 6.0, the surface of AWDBC becomes negatively charged, making it challenging to adsorb negatively charged HA. Uranium uptake would be reduced as a result of the HA molecule in aqueous solution forming complexes (HA-U) with uranium ions. As a consequence, the effect of co-existing pollutant findings showed that at pH less than 4.0, uranium uptake was unaffected by humic acid, while at pH greater than 7.0,

uranium uptake dramatically heightened as humic acid concentration surged [98].

In another study, the effect of competing monovalent, divalent, and trivalent ions as well as radionuclide isotopes was assessed on the adsorption of U^{6+} using Calcium phosphate-modified cotton straw and calcium phosphate-modified microbial etch cotton straw biochar. The findings showed that because of their poor Coulomb interaction and lower ionic charge to U^{6+}, K^{+}, Cu^{2+}, Mn^{2+}, Cs^{+}, and $Sr^{+,}$ decreased the uranium adsorption by 45.3%, 55.7%, 12.1%, 33.2%, and 46.8%, respectively. On the other hand, because Fe^{3+} had a lower ionic radius and a higher valence, which made it more combative for binding to the surface sites, it greatly hampered uranium adsorption by reducing it by 98%. These outcomes connote that the adsorption effectiveness of the AWDBC may be considerably impacted by the existence of certain ions in actual radioactive wastewater. Therefore, for effective uranium cleanup from wastewater, more adsorption process optimization could be required [81].

6. Adsorption isotherm modelling

One of the most important considerations when designing an adsorption technology is the adsorption isotherm [7,106]. It plays a critical role in adsorption studies, providing insight into the interactions between adsorbate (uranium) and agrogenic waste-derived biochar (adsorbent). More so, the distribution of the uranium on the AWDBC is shown using isotherm modeling [107]. It also aids in emphasizing the biochar's porous character and is predicated on the adsorbate-adsorbent assumptions. In addition, it is useful in figuring out the biochar sorption capacity and making the most of its application in the most effective adsorption method [7].

More than a few studies have explored the adsorption isotherm modeling of uranium radio-pollutant on various agrogenic waste-derived biochars. Notably, as presented in Table 2, various isotherm models including the Redlich–Peterson isotherm (RPI) model, Dubinin-Radushkevic isotherm (DRI) model, Temkin isotherm (TI) model, Langmuir isotherm (LI) model, Sips isotherm model, and Freundlich isotherm (FI) model have been applied for the adsorption of uranium onto AWDBC [68,71,77,92,94]. Interestingly, based on various R^2 readings (correlation coefficient), a larger percentage of the studies under consideration reported Langmuir as the best-fit isotherm model with R^2 readings spanning from 0.91 to 0.9993 [88,94,101]. The Langmuir classical model and its allied FI model, which has two parameters, are still the most theoretically straightforward types of isotherm models. They are also very easy to implement and require less computational and statistical work [107]. For instances where LI is reported as the best isotherm to describe the sequestration of uranium, the agrogenic waste-derived biochar surface adsorption sites are said to be equally available and energetically homogeneous, and the sequestration may be considered to be occurring in monolayers with no interaction between the uranium adsorbate ions [68,69,74,76,95,97]. In addition to this, Wang et al., accentuated that this scenario might be ascribed to the biochar's uniform distribution of surface functional groups, which promotes chemical adsorption [81]. More so, the unapplicable isotherm model can also be used to predict one or two things about the adsorption operation and thus cannot be totally discarded. For example, in the adsorption of uranium using camphor tree leaves biochar, three isotherm models were applied (TI, LI, and FI), and Langmuir was confirmed to be the best fit ($R^2 = 0.9993$) among them. However, the authors were able to use the Temkin to predict that the adsorption operation is endothermic in nature, as it was observed that the heat of capture surges with an upsurge in temperature [94]. Similarly, in another experiment using *Salvadora persica* branches biochar, Albayari et al., used Temkin to predict that the adsorption operation is exothermic, even though the adsorption isotherm of best fit is Langmuir [95]. In another study, Langmuir was reported as the best fit using bamboo powder@ MoS_2-PO_4 and bamboo powder@ MoS_2 biochar among three applied isotherm models (Langmuir, D-R, and Freundlich). Nevertheless, DRI which was unfit was used by the authors to predict that the uranium sorption operation is chemisorption because the adsorption energy parameter of the DRI falls between 8 and 16 kJ/mol and on a general note, when the DRI sorption energy is < 8 kJ/mol, physisorption is suggested to be at play, otherwise, if the energy is > 8 to <16 kJ/mol, then chemisorption is at play [71,77,92]. Furthermore, there are two cases where two isotherm models (Sips and RPI) were reported to be the best fit for uranium adsorption [71,79]. However, the mystery behind this kind of phenomenon was not expounded by the authors. Nevertheless, from our own point of view, we think the diversity in the pore architecture and active site energy of the biochar is responsible for this. Moreover, the two models in question are similar in nature. Specifically, in the adsorption system, the RPI and Sips models show a combinatory and interfacing between heterogeneous and homogeneous features. Because of this versatility, the models explain the equilibrium of adsorption across a wide concentration spectrum (high and low), fitting both LI and FI characteristics [64]. Also, when the FI is the best fit or part of the best-fit isotherm model, it suggests multilayer uranium adsorption and predicts a vast number of

Table 2. Summary of isotherm modeling of uranium sequestration by agrogenic waste biochar.

Agrogenic waste biochar	Applied isotherm model	Best-fit	R^2	Ref.
Peanut shells@MnO	LI, FI, and Sips	LI	0.997	[82]
Litchi shell	LI and FI	FI	0.991	[100]
Peanut shells	LI, FI, and Sips	LI	0.995	[82]
Durian shells	LI and FI	LI	0.99	[86]
Corn straw @ZVMn	LI and FI	LI	0.983	[89]
Peanut shell@Fe-Ni	LI and FI	LI	0.95	[90]
Hami-melon peels	LI and FI	LI	0.98	[93]
Apple tree branches@$MnFe_2O_4$	LI and FI	FI	0.99	[96]
Lotus seedpods	LI and FI	LI	0.9789	[72]
Rice straw	DRI, LI, RPI, FI, and Sips	Sips and RPI	0.98 and 0.96	[71]
Reed straw	LI and FI	LI	0.9906	[99]
Fish scales	LI and FI	LI	0.873	[88]
Bamboo powder@MoS_2	LI, DRI, and FI	LI	0.974	[92]
Cow manure	LI and FI	LI	0.979	[68]
Orange peel	DRI, LI, RPI, FI, and Sips	Sips and RPI	0.989	[77]
Orange peel@magnesium silicate	TI, LI and FI	LI	0.991	[76]
Salvadora persica branches	TI, LI, and FI	LI	0.9968	[95]
HNO_3-modified Cow manure	LI and FI	LI	0.958	[68]
Fe_3O_4@pine needles	LI	LI	0.992	[80]
Magnetized watermelon rind	TI, LI, and FI	LI	0.99	[87]
Rice husk@Fe_2O_3	LI and FI	LI	0.9897	[98]
Lotus seedpods@NH_2	LI and FI	LI	0.9898	[72]
Horse manure	TI, LI, and FI	LI	0.998	[74]
Citrullus lanatus L. seeds@$MnFe_2O_4$	LI and FI	LI	0.96	[101]
Bamboo powder@ MoS_2-PO_4	LI, DRI and FI	LI	0.996	[92]
Wheat straw	LI and FI	LI	0.975	[68]
Luffa rattan	LI and FI	LI	0.991	[85]
Rice straw (Oxidized)	DRI, LI, RPI, FI, and Sips	Sips and RPI	0.99	[71]
Citrullus lanatus L. Seeds	LI and FI	LI	0.91	[101]
Wheat straw	LI and FI	LI and FI	>0.98	[79]
H_2O-modified pig manure	LI, RPI, FI, and Sips	LI	0.994	[75]
Pine needles	LI and FI	LI	0.99	[97]
KOH-activated fish scales	LI and FI	LI	0.91	[88]
H_2O_2-modified pig manure	LI, RPI, FI, and Sips	LI	0.997	[75]
Bamboo residues@polyethyleneimine@NaOH	LI and FI	LI	0.998	[69]
Cotton straw	LI and FI	LI	0.965	[81]
$KMnO_4$-modified pig manure	LI, RPI, FI, and Sips	LI	0.996	[75]
HNO_3-modified wheat straw	LI and FI	LI	0.985	[68]
Camphor tree leaves	TI, LI, and FI	LI	0.9993	[94]
Watermelon rind	TI, LI and FI	LI	0.99	[87]
Horse manure@Bi_2O_3	TI, LI, and FI	LI	0.994	[74]
Bamboo residues@polyethyleneimine@HNO_3	LI and FI	LI	0.983	[69]
Orange peel@MnO_2	DRI, LI, RPI, FI, and Sips	Sips and RPI	0.997	[77]
Coconut shell@ $Ti_3C_2T_x$ and @polydopamine@ polyethyleneimine	LI and FI	LI	0.982	[78]

parallel adsorption spots with various adsorption-free energies [64,79]. The heterogeneous biochar surface where the adsorption process takes place suggests that the binding spots are not equivalent [64,99].

7. Adsorption kinetic modeling

Kinetic modeling is employed to ascertain the adsorption rate constant [107]. Specifically, the study of adsorption kinetics entails examining the rate at which the adsorbate is absorbed, providing insight into how reactant concentration affects the speed of reaction. This speed basically determines how long the adsorbate stays at the solid-liquid phase contact, which makes it easier to formulate/forecast the mechanism of reaction using theoretical models. More specifically, the rate of adsorption is a critical factor in evaluating the efficacy of an adsorbent. Moreover, kinetic studies can be used to identify intermediates and transition states [64]. More so, the impact of biochar dose and uranium concentration on the adsorption process can be better understood by looking at the kinetic behavior of the process [7]. Moreover, based on the preliminary presumptions of the kinetics of best-fit models, some insight into the adsorption mechanism is obtained [107].

Several studies have explored the adsorption kinetics modeling of uranium radio-pollutant on various agrogenic waste-derived biochars. Notably, as presented in Table 3, various kinetic models, including pseudo-first-order (PFO), pseudo-second-order (PSO) [69], Elovich model, and intra-particle diffusion (IPD), have been applied for the adsorption of uranium onto AWDBC [78,94,101]. Interestingly, based on various R^2 readings (correlation coefficient), all the studies under consideration reported PSO as the best-fit kinetics model except for the adsorption of uranium using fish scale biochar and KOH-activated fish scale biochar which is reported to follow the PFO model with R^2 value close to 1 (0.968 and 0.980 respectively) [88]. The author suggests that based on the PFO best fit, the uranium uptake is governed by the chemisorption mechanism, and it is also that was the rate-determining/controlling mechanism of the adsorption operation [88]. For the PSO, it hypothesized that the adsorption of the uranium is governed by chemisorption. Additionally, it is assumed that the concentration of the uranium radio-pollutant and the dose of the AWDBC, which is measured as the number of available active sites, have an impact on the process's kinetics [7]. Furthermore, the fitting of uranium adsorption data into kinetic models affords information on uranium time dependency (the least amount of time required for substantial adsorption to take place) and the potential

Table 3. Overview of adsorption kinetic modeling of uranium sequestration by agrogenic waste biochar.

Agrogenic waste biochar	Applied kinetic model	Best-fit	R^2	Ref.
Durian shells	PFO and PSO	PSO	0.998	[86]
Peanut shells@MnO	Elovich, PFO, PSO, and IPD	PSO	0.999	[82]
Litchi shell	PFO and PSO	PFO	0.998	[100]
Peanut shells	Elovich, PFO, PSO, and IPD	PSO	0.997	[82]
Corn straw @ZVMn	PFO, PSO, and Temkin	PSO	0.993	[89]
Hami-melon peel	PFO, PSO, and IPD	PSO	0.9998	[93]
Peanut shell@Fe-Ni	PFO, PSO, and Weber–Morris	PSO	0.999	[90]
Apple tree branches@$MnFe_2O_4$	PFO, PSO, and IPD	PSO	0.99	[96]
Lotus seedpods	PFO, PSO, and IPD	PSO	0.9558	[72]
Rice straw	PFO, PSO, and IPD	PSO	0.99	[71]
Reed straw	PFO and PSO	PSO	0.9586	[99]
Fish scales	PFO and PSO	PFO	0.968	[88]
Bamboo powder@MoS_2	PFO, PSO, and IPD	PSO	0.970	[92]
Cow manure	PFO and PSO	PSO	0.999	[68]
Orange peel	PFO, PSO, and IPD	PSO	0.99	[77]
Orange peel@magnesium silicate	PFO, PSO, and Elovich	PSO	0.998	[76]
Salvadora persica branches	PFO and PSO	PSO	1	[95]
HNO_3-modified Cow manure	PFO and PSO	PSO	0.999	[68]
Fe_3O_4@pine needles	PFO and PSO	PSO	0.99	[80]
Macaúba endocarp	Elovich, PFO, PSO, and IPD	PSO	0.999	[84]
Magnetized watermelon rind	PFO and PSO	PSO	0.999	[87]
Rice husk@Fe_2O_3	PFO, PSO, and IPD	PSO	>0.99	[98]
Lotus seedpods@NH_2	PFO, PSO, and IPD	PSO	0.9676	[72]
Horse manure	Elovich, PFO, and PSO	PSO	0.999	[74]
Citrullus lanatus L. seeds@$MnFe_2O_4$	PFO and PSO	PSO	0.96	[101]
Bamboo powder@ MoS_2-PO_4	PFO, PSO, and IPD	PSO	0.999	[92]
Luffa rattan	PFO and PSO	PSO	1.00	[85]
Rice straw (Oxidized)	PFO, PSO, and IPD	PSO	0.98	[71]
Citrullus lanatus L. Seeds	PFO and PSO	PSO	0.85	[101]
Wheat straw	PFO and PSO	PSO	0.9599	[79]
H_2O-modified pig manure	PFO and PSO	PSO	0.970	[75]
Pine needles	PFO and PSO	PSO	0.993	[97]
KOH-activated fish scales	PFO and PSO	PFO	0.980	[88]
H_2O_2-modified pig manure	PFO and PSO	PSO	0.987	[75]
Bamboo residues@polyethyleneimine@NaOH	IPD and PSO	PSO	0.999	[69]
Cotton straw	PFO and PSO	PSO	0.980	[81]
$KMnO_4$-modified pig manure	PFO and PSO	PSO	0.979	[75]
Camphor tree leaves	PSO, IPD, and Elovich	PSO	0.9978	[94]
Watermelon rind	PFO and PSO	PSO	0.989	[87]
Horse manure@Bi_2O_3	Elovich, PFO, and PSO	PSO	0.999	[74]
Bamboo residues@polyethyleneimine@HNO_3	IPD and PSO	PSO	0.998	[69]
Orange peel@MnO_2	PFO, PSO, and IPD	PSO	0.99	[77]
Coconut shell@ $Ti_3C_2T_x$ and @polydopamine@ polyethyleneimine	PFO, Elovich, PSO, and IPD	PSO	0.98	[78]

process by which uranium diffuses from the bulk solution to the surface of the biochar. For instance, a study of U(VI) adsorption at varying residence times using lotus seedpods and NH_2 functionalized lotus seedpods biochar. It is evident that after 60 min, lotus seedpods and lotus seedpods@NH_2 were able to sustain a high U(VI) adsorption rate. While the U(VI) adsorption capacity of lotus seedpods@NH_2 achieved saturation after 240 min, that of lotus seedpods reached saturation at 60 min and subsequently stayed constant. The author stated that this resulted in smaller pores and a longer equilibrium period because, following amino functionalization, the NH_2 groups occupied the pore location, restricting the flow of uranyl ions in the solution. Furthermore, the adsorption data was confirmed to fit the PSO kinetic model which signifies that chemisorption was the chief adsorption mechanism [72]. Similarly, for the adsorption of uranium using reed straw biochar, the adsorption was reported to surge very fast in the first 1 h, and progressively attained equilibrium after 6 h. The author opined that the sorption reaction is chemisorption since the kinetic data fitted PSO than PFO [99]. In another experiment [71], the impact of contact time on uranium sequestration by rice straw and oxidized rice straw biochar was explored. For rice straw biochar, a quick equilibrium phase was seen in the first 30 min of the experiment, followed by a long equilibrium phase for oxidized rice straw biochar. The presence of adequate active spots and a larger uranium concentration gradient were attributed to the fast growth phases [71]. In addition, the adsorption gradually attaining equilibrium might be because as the reaction evolves, the sorption spots on the surface of the biochar are increasingly roofed by U(VI) [85]. Moreover, the U(VI) dynamics were examined using IPD, PSO, and PFO models and it was found that PSO best describes the adsorption process among the three kinetic models employed. The IPD model frequently provides an explanation for the mobility of microparticles inside the adsorbent material. The exterior surface diffusion or quick (instantaneous) adsorption and the relatively sluggish IPD, which reaches zero at equilibrium, are indicated by the declining order of the diffusion rate constants. This is a rate-controlling step in the whole adsorption process, suggesting that strong surface complexation or chemical adsorption, rather than mass transfer, is mostly responsible for controlling the U(VI) sequestration by biochar [71]. This is in parallel with the governance of surface complexation/chemisorption process reported for uranium uptake by rice husk@-Fe_2O_3 BC and modified pig manure biochar [75,98]. Albayari and co-workers also confirmed PSO with a perfect R^2 (1.0) and chemisorption mechanism for the adsorption of uranium using *Salvadora persica* branches biochar [95]. This is consistent with other studies that have reported PSO model and chemisorption through e− exchanging/sharing between uranium and biochar, accompanying valence forces [68,69,74,77,79,81,92,94,97,101].

8. Thermodynamic modeling

This section discusses the thermodynamic modeling of agrogenic waste-derived biochar adsorption of uranium radio-pollutant as a crucial index for judging the spontaneity and feasibility of adsorption technology for industrial scaling-up prediction. The measurement of the change in Gibbs free energy (ΔG^0), entropy (ΔS^0), and enthalpy (ΔH^0) typically clarifies the thermodynamics of adsorption [107–112]. These are calculated by the system of equations presented by Emmanuel's research group [7]. Table 4 presents the thermodynamics overview of the AWDBC uranium sorption. Notably, all the ΔG^0 readings were negative (less than zero), indicating that uranium adsorption was spontaneous [71,99]. More specifically, the majority of uranium adsorption systems are spontaneous under ambient and near-ambient conditions (10–60 °C) as uniform physical interactions can be realized between agrogenic waste-derived biochar and the uranium radio-pollutant at these conditions. According to Igwegbe and co-workers, when the adsorbate is able to overcome the mass transfer constraint at the solid-liquid interphase without the assistance of an external component, spontaneity is accomplished [107]. In addition, an attenuation in ΔG° value with an upsurge in temperature demonstrates that uranium sequestration is thermodynamically favorable on the AWDBC at elevated temperatures for all the reported studies [71,81]. Except for Wang et al., that argued in their study that the ΔG° value for HNO_3 and NaOH-modified bamboo residues@polyethyleneimine BC surges as the temperature surges, signifying that low temperature is advantageous for uranium adsorption [69]. This contradiction corroborates the opinion of Igwegbe et al. that the van't Hoff equation has flaws when applied without giving the idea of physical chemistry of equilibrium more thought [107].

Furthermore, uranium adsorption can be either exothermic or endothermic, subject to the characteristics of the agrogenic waste-derived biochar as dictated by the sign of the readings of ΔH^0 [69,79,97]. As shown in Table 4, all the reported studies show endothermic (ΔH^0 above zero) adsorption operation which means heat is absorbed from the surroundings during the reaction except for *Salvadora persica* branches BC and $NaOH/HNO_3$ modified bamboo residues@polyethyleneimine BC where ΔH^0 below zero was reported, signifying exothermic (release of heat to the

Table 4. Summary of thermodynamics modeling of uranium sequestration by agrogenic waste biochar.

Agrogenic waste biochar	Temp (°C)	ΔG^0	ΔH^0 (J/mol)	ΔS^0 (kJ/mol.K)	References
Rice straw	15	−17.13	32.94	172.78	[71]
	20	−18.21			
	25	−19.36			
	30	−20.15			
	40	−21.37			
Reed straw	10	−12.65	33.76	0.16480	[99]
	25	−15.11			
	40	−17.57			
	55	−20.03			
Bamboo powder@MoS_2	15	−23.57	17.27	0.14171	[92]
	25	−24.98			
	35	−26.40			
	45	−27.82			
Orange peel	15.15	−16.64	33.33	0.17343	[77]
	20.15	−17.51			
	25.15	−18.38			
	30.15	−19.25			
	40.15	−20.98			
Orange peel@magnesium silicate	25	−40.223	16.801	0.19153	[76]
	35	−42.277			
	50	−45.029			
Salvadora persica branches	25	−12.17	−218.17	−0.69	[95]
	35	−8.71			
	45	−5.26			
	40	−1.80			
Magnetized watermelon rind	20	−2.02	14.35		[87]
	30	−2.79			
	40	−3.23			
	50	−3.74			
Rice husk@Fe_2O_3	15	−3.79	2.68	0.02243	[98]
	30	−5.15			
	45	−7.55			
Citrullus lanatus L. seeds@$MnFe_2O_4$	25	−24.13	23.63	0.17	[101]
	30	−25.89			
	45	−27.45			
Bamboo powder@ MoS_2-PO_4	15	−25.92	21.95	0.16611	[92]
	25	−27.58			
	35	−29.24			
	45	−30.90			
Luffa rattan	25.15	−6.74	14.88	0.072514	[85]
	35.15	−7.46			
	45.15	−8.19			
Rice straw (Oxidized)	15	−14.04	58.26	247.41	[71]
	20	−15.17			
	25	−16.34			
	30	−18.27			
	40	−20.08			
Wheat straw	20	−31.89	36.28	0.10884	[79]
	40	−34.07			
	60	−36.24			
Pine needles	15	−12.7	36.1	0.1697	[97]
	25	−14.4			
	35	−16.1			
	45	−17.8			
	55	−19.5			
Bamboo residues@polyethyleneimine@NaOH	25	−6.60	−25.79	−0.06551	[69]
	40	−5.47			
	55	−4.52			
Cotton straw	10.16	−3.40	5.45	0.00723	[81]
	20.16	−3.34			
	30.16	−3.26			
	40.16	−3.18			
Bamboo residues@polyethyleneimine@HNO_3	25	−5.06	−21.80	−0.05592	[69]
	40	−4.37			
	55	−3.40			

(*continued on next page*)

Table 4. (continued)

Agrogenic waste biochar	Temp (°C)	ΔG^0	ΔH^0 (J/mol)	ΔS^0 (kJ/mol.K)	References
Orange peel@MnO_2	15.15	−13.49	57.67	0.24697	[77]
	20.15	−14.73			
	25.15	−15.96			
	30.15	−17.20			
	40.15	−19.67			
Coconut shell@ $Ti_3C_2T_x$ and @polydopamine@ polyethyleneimine	25	−11.57	3.291	0.04988	[78]
	40	−12.33			
	60	−13.32			

surrounding) adsorption process [69,95]. The kind of chemical reaction taking place between the uranium radio-pollutant and agrogenic waste-derived biochar is also revealed by the ΔH^0 change. For example, Albayari et al. accentuated in a study of uranium adsorption using *Salvadora persica* branches BC that −218.17 kJ mol^{-1} ΔH^0 value obtained indicates an exothermic adsorption operation and suggests that the chemisorption mechanism governs the adsorption operation which is elucidated by the forces of interaction between the biochar and uranium, which are greater than those present in both biochar and uranium individually, which means that it would prefer the product over reactant [95]. In addition, quality information on the adsorption system's disorderliness at the solid-liquid interface and how it varies during the adsorption process may be extracted from the change in ΔS^0 reading. Interestingly, from the data presented in Table 4, it can be noted that ΔS^0 greater than zero, associated with a randomness upsurge at the solid-liquid interface, was observed for all the studies under consideration. This randomness upsurge phenomenon might be due to the solid-solution mass transfer interface during the adsorption process [71]. Conversely, the presence of a negative ΔS^0 reading suggests that there is no structural change at the solid-liquid interface and that randomness reduces with uranium adsorption [69,95]. In conclusion, the remarkable spontaneity of the uranium adsorption process can be ascribed to the distinguished physico-chemical characteristics of agrogenic waste-derived biochar, which enhanced the adsorption capacity. These characteristics include a high pore size, a large SSA, and an abundance of active functional groups [78].

9. Biochar reclamation, regeneration, and reusability

Without adsorbent, there is nothing called adsorption technology. However, the scalability and stability of an adsorbent, which is part of the crucial index that determines the industrial practicality and eco-economic viability of adsorption technology, are contingent on the reusability of the adsorbent in question [69,70,113−115]. As depicted in Fig. 10, the reusability involves the recovery of the exhausted adsorbent from the reaction mixture, desorption of adsorbed adsorbate from the recovered adsorbent, and or the regeneration of the recovered spent adsorbent to restore its innate integrity to use it again in another round of adsorption experiment. Notable works in this direction on the adsorption of uranium radio-pollutant using agrogenic waste-derived biochar are empirically discussed in the next paragraphs and summarily presented in Table 5.

For example, in the adsorption process of U(VI) using phosphorus-doped pomelo peel biochar, regeneration and reusability experiments were conducted [70]. In this research, the exhausted biochar was regenerated by eluting with 0.5 M HNO_3 solution. In the procedure, the biochar integrity was restored once the sorbed U(VI) ions were liberated from the adsorption sites. After a single usage, biochar may be effectively regenerated, as seen in Table 5. Since the U(VI) desorption degree stays over 97%, almost all of the U(VI) that has been adsorbed from biochar has been liberated. Furthermore, phosphorus-doped pomelo peel biochar can go through at least five rounds of adsorption and desorption without seeing a drop in either adsorption or desorption efficiency. Throughout the desorption-adsorption cycle, the desorption efficiency remains over 95%, and the U(VI) sequestration efficiency of the regenerated phosphorus-doped pomelo peel biochar remains above 97% [70]. In another study, using an adsorption-desorption experiment, the stability and reusability of Bamboo residues@polyethyleneimine@NaOH and Bamboo residues@polyethyleneimine@HNO_3 BC were assessed [69]. The respective spent BC was rinsed with 0.01 M HCl following adsorption, and the solution was agitated for 12 h to promote desorption. After centrifuging the biochar-containing solution, it was rinsed three times with deionized H_2O and then freeze-dried. The following round of U(VI) adsorption study then made use of the dry regenerated biochar. Five times, the adsorption-desorption cycle was repeated. According to Table 5, both biochars exhibit a little drop in adsorption rates of around 10−12%. These findings show that Bamboo residues@polyethyleneimine@NaOH and Bamboo residues@polyethyleneimine@HNO_3 BC are both viable and

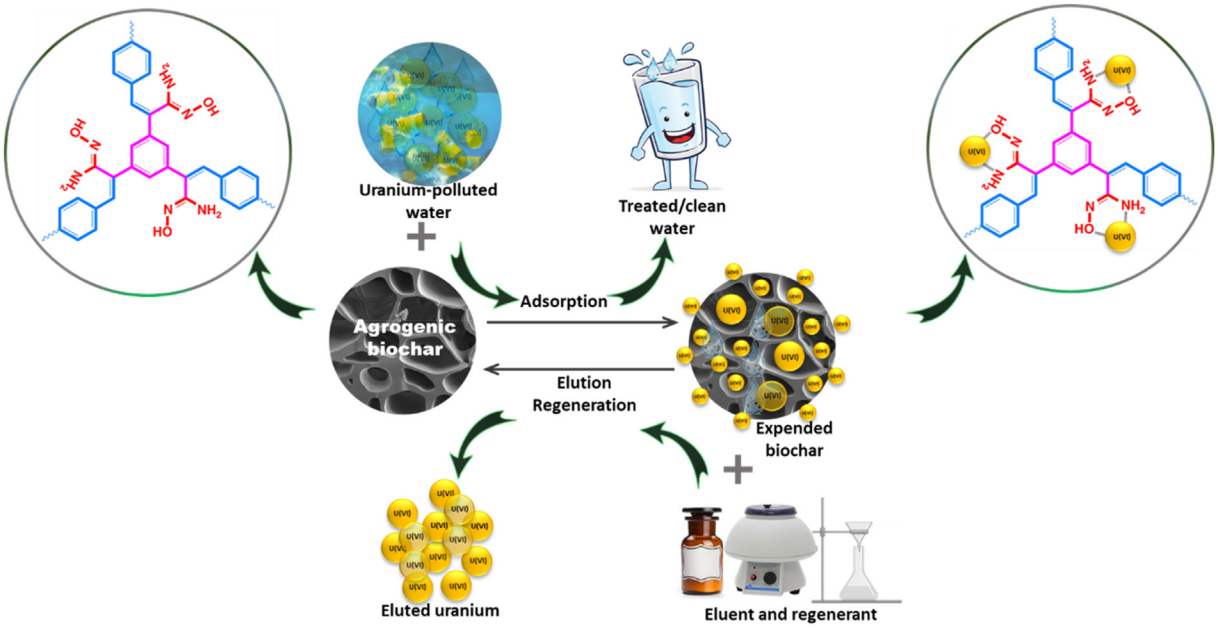

Fig. 10. Overview of adsorption-desorption. Modified from Refs. [7,116].

Table 5. Summary of adsorption-desorption studies.

Agrogenic waste biochar	Eluent/ Regenerant	Percentage (%) removed (1st round)	No. of round	Percentage (%) removed (nth round)	References
Rice straw	1.0 M HCl	95	5	>90	[71]
Fe_3O_4@pine needles	0.1 M Na_2CO_3	99.6	4	62.6	[80]
Watermelon rind@ Fe_3O_4	0.1 M Na_2CO_3	99	3	44	[87]
Citrullus lanatus L. seeds@$MnFe_2O_4$	0.5 M HCl	>80	5	>60	[101]
Pine needles	0.05 M HCl	99.11	4	88.37	[97]
KOH-activated fish scales	HCl	94	5	83	[88]
Bamboo residues@polyethyleneimine@NaOH	0.01 M HCl	>85	5	>75	[69]
Cotton straw	0.1 M Na_2CO_3	98	6	96	[81]
Bamboo residues@polyethyleneimine@HNO_3	0.01 M HCl	>80	5	>66	[69]
Phosphorus-doped pomelo peel	0.5 M HNO_3	>97	5	>97	[70]
Orange peel@MnO_2	1.0 M HCl	~100	5	~95.60	[77]
Coconut shell@ $Ti_3C_2T_x$ and @polydopamine@ polyethyleneimine	1 M HCl	~90	4	>75	[78]
Cow manure@ TiO_2@SiO_2	0.05 M HCl	>90	5	>87.6	[73]
Citrullus lanatus L. seeds	0.5 M HCl	>60	5	<40	[101]
Fish scales	HCl	72	5	60	[88]
Cotton straw	1 M Na_2CO_3	98	6	87	[81]

affordable materials with good stability and reusability [69]. In the same spirit, the elution of U(VI) from *Citrullus lanatus* L. Seeds and *Citrullus lanatus* L. seeds@$MnFe_2O_4$ BC was performed through the HCl desorption [101]. In this investigation, *Citrullus lanatus* L. Seeds' biochar regeneration showed comparatively poorer performance in contrast to its $MnFe_2O_4$ composite, as shown in Table 5. Seeds and *Citrullus lanatus* L. seeds@$MnFe_2O_4$ biochar demonstrated comparatively high effectiveness towards U(VI) sequestration (60–80%) even after five regeneration rounds. Because of this, the results suggest that Seeds and *Citrullus lanatus* L. seeds@$MnFe_2O_4$ biochar have a strong chance of functioning as an environmentally benign adsorbent for the sequestration of U(VI) from aqueous media [101]. A somewhat remarkable reusability efficiency was also reported for the adsorption-desorption of U(VI) using Watermelon rind@ Fe_3O_4, Fe_3O_4@pine needles, and rice straw biochar as presented in Table 5 [71,80,87].

In another study, the regenerability of spent KOH-activated fish scales and fish scales biochar was performed to evaluate the reusability potential for U(VI) sequestration [88]. Following five regeneration experiment cycles, there was a small decline in the

adsorption efficiency; specifically, the percentage of fish scale biochar and KOH-activated fish scale biochar elimination reduced from 72 to 60% and from 94 to 83%, respectively. As the adsorption-desorption rounds continue, the mass loss of the biochar during the runs may be responsible for the slight decline in adsorption capacity for KOH-activated fish scale biochar. On the other hand, the larger reduction in adsorption capacity for fish scale biochar may be explained by the fact that U(VI) was not desorbed by HCl and continued to occupy a certain percentage of the adsorption sites. On this note, it can be inferred that KOH-activated fish scale biochar showed great promise as an adsorbent candidate for extended usage [88]. Similarly, Zhang et al. studied the expended pine needles' biochar desorption efficiency was assessed using a 0.001−0.1 M HCl solution [97]. The findings showed that the sequestrated U(VI) could be totally eluted from the expended pine needles biochar using 0.05 M HCl. As a consequence, the adsorption-elution sequence was executed four times using the same AWDBC and 0.05 M HCl to examine the regeneration characteristics. It was evident that following four rounds, the initial values of the uptake capacity, elimination, and elution ratio were 50.17 mg/g, 99.11% and 96.03%, and 45.41 mg/g, 88.37% and 87.41%, respectively. Thus, the pine needles biochar may be efficiently regenerated using a 0.05 M HCl solution [97].

10. Knowledge gaps, challenges, and areas for future study

Herein, research gaps, limitations, and future research hotspots were presented to inform future researchers on possible aspects of the research to improve in the field.

Notably, a significant amount of research has focused on artificial uranium radio-polluted water formulated in the laboratory instead of effluent from the real-life scenario site. Because AWDBC is a highly effective adsorbent, pollutants found in industrial effluents are adsorbed competitively at its surface. This leads to pore blockages, obstructions in the pore filling, and processes that resemble intraparticle diffusion, and this hinders uranium uptake by biochar [117]. Therefore, it is necessary to thoroughly evaluate the usage of agrogenic waste-derived biochar and its composites in wastewater from the real-life scenario location. Field uranium wastewater should be used instead of artificially formulated uranium wastewater in future scientific investigations.

Also, the paucity of studies on the financial analysis and scalability of uranium adsorption in water resource management systems is another significant research vacuum. Although the theoretical possibilities of these systems are explored, it is still unclear what effect they will have on the environment in a real-life scenario. To put these systems into practice, future researchers need to look at column adsorption studies that simulate real-world settings in addition to batch adsorption studies.

Furthermore, the study found that agrogenic waste-derived biochar can be recovered and recycled, notwithstanding there was a sharp decline in recovery percentage at higher cycles (often $n > 3-6$). In the future, investigating more effective biochar modification techniques or superior eluting agents that may enable the AWDBC to operate better in this context is crucial. This is essential; otherwise, agrogenic waste-derived biochar would not be useful for any kind of industrial or real-world application.

One other important finding is that research that indicates multiple usages does not have consistent standards for ending reuse cycles. Given that some AWDBCs continue to have substantial absorption capacity even after reuse cycles end, this discrepancy makes it difficult to draw meaningful comparisons between various AWDBCs. We recommend extending reuse cycles until the uranium sorption falls to a predefined level (e.g., <50 % uptake efficiency) in order to obtain a more precise evaluation and to provide more accurate comparisons.

Additionally, there is no report on the application of artificial intelligence (AI) and statistical physics modeling to look into the energy of interactions and determine the possible mechanism of adsorption [107] of agrogenic waste-derived biochar for uranium radiopollutants. This is an eye-catching research gap that offers a fascinating chance to use such potent computational techniques for environmental issue-solving.

Lastly, a crucial aspect that has been largely ignored in existing studies is the disposal of recycled spent AWDBC even after multiple reuses. In the future, researchers working in this area need to investigate and devise practical solutions for this problem in order to guarantee a thorough and long-lasting approach to environmental remediation.

11. Conclusion

Summarily, this review study revealed that agrogeinc waste-derived biochar and adsorption technique is a suitable option for the purification of uranium radiopolluted water, offering high adsorption capacities of up to 1527.02 mg/g. In addition, numerous key values and major findings were derived from this study, which also suggest the suitability of agrogenic waste-derived biochar for uranium cleanup in an aqueous environment. Firstly, it was found that the AWDB has a high surface area of up to 1521.38 m^2/g, particularly for

phosphorus-doped pomelo peel biochar, which contributed to high uranium removal efficiency.

Secondly, the study also revealed that modified AWDBC performed better than unmodified ones due to their distinguished physicochemical characteristics like good specific surface area, better porosity, and the presence of an abundance of active sites and functional groups like hydroxyl, carboxyl, and amine groups. Thus, a major advantage of AWDBC exploration is the possibility of doping/modifying them with other materials to improve the adsorption efficiency under different conditions. Nevertheless, from the pH study, it was deduced that both modified and unmodified AWDBC can work well in harsh environments within >2 and <8 pH.

Furthermore, it was discovered from this review work that AWDBC has good reusability potential up to 6 adsorption-desorption rounds with an average uranium cleanup efficiency of >70% in most cases at the nth cycle, which confirms the excellent stability and structural integrity of the biochar. Moreover, it was found that Na_2CO_3 and HCl are better eluents for desorbing uranium from spent AWDBC.

Also, it was revealed that the best-fit isotherm and kinetic modeling are the classic Langmuir and PSO models with R^2 close to unit (1.0). This establishes that the concentration of the uranium radio-pollutant and the dose (5–100 mg) of the BWDBC, which is measured as the number of available active sites, have an impact on the adsorption process's kinetics The analysis of thermodynamics shows that most of the adsorption operations are endothermic and spontaneous processes with a disorder upsurge at the solid-liquid interface. Additionally, from the mechanism angle, electrostatic interactions, π-π interactions, pore diffusion, and complexation through available functional groups govern the uranium sequestration operation.

By and large, this review work shows that the use of agrogeinc waste-derived biochar for the adsorption of uranium from wastewater contributes to sustainable agricultural practices, solid waste management, circular economy advancement, SDG 6, 12, and 14 actualizations, and promotes water remediation as well as environmental sustainability in a world increasingly reliant on nuclear technology. Ultimately, for process optimization, the study of expended biochar disposal, the use of AI and statistical physics modeling techniques, the enhancement of biochar desorption, and financial analysis are suggested as areas for possible future work.

Data availability statements

Data sharing is not applicable to this article as no datasets were generated or analyzed during the current study.

Funding

No funds, grants, or other support was received.

Conflicts of interest

The authors don't have any financial or non-financial conflict of interest to declare.

References

[1] P.L. Smedley, D.G. Kinniburgh, Uranium in natural waters and the environment: distribution, speciation and impact, Appl. Geochem. 148 (2023) 105534, https://doi.org/10.1016/j.apgeochem.2022.105534.
[2] K. Sanyal, S. Dhara, Recent advances in ultra-trace determination of uranium in natural water using total reflection X-ray fluorescence (TXRF) spectrometry, X Ray Spectrom. 53 (2023) 326–339.
[3] B.M.T. Costa Peluzo, E. Kraka, Uranium: the nuclear fuel cycle and beyond, Int. J. Mol. Sci. 23 (2022) 4655.
[4] P. Miśkowiec, Name game: the naming history of the chemical elements—part 1—from antiquity till the end of 18th century, Found. Chem. 25 (2023) 29–51.
[5] A. Vengosh, R.M. Coyte, J. Podgorski, T.M. Johnson, A critical review on the occurrence and distribution of the uranium-and thorium-decay nuclides and their effect on the quality of groundwater, Sci. Total Environ. 808 (2022) 151914.
[6] G. Bjørklund, Y. Semenova, L. Pivina, M. Dadar, M.M. Rahman, J. Aaseth, et al., Uranium in drinking water: a public health threat, Arch. Toxicol. 94 (2020) 1551–1560.
[7] S.S. Emmanuel, A.A. Adesibikan, A.A. Bayode, C.O. Olawoyin, E.J. Isukuru, O.Y. Raji, A review on covalent organic frameworks with Mult-site functional groups as superior adsorbents for adsorptive sequestration of radio-contaminants, J. Organomet. Chem. 1015 (2024) 123226, https://doi.org/10.1016/j.jorganchem.2024.123226.
[8] J.O. Ighalo, Z. Chen, C.R. Ohoro, M. Oniye, C.A. Igwegbe, I. Elimhingbovo, et al., A review of remediation technologies for uranium-contaminated water, Chemosphere 352 (2024) 141322, https://doi.org/10.1016/j.chemosphere.2024.141322.
[9] G.S. Jones, Reactor-grade plutonium and nuclear weapons: ending the debate, Nonproliferation Rev. 26 (2019) 61–81.
[10] J.A. Kazery, G. Proctor, S.L. Larson, J.H. Ballard, H.M. Knotek-Smith, Q. Zhang, et al., Distribution and fractionation of uranium in weapon tested range soils, ACS Earth Space Chem. 5 (2021) 356–364.
[11] N. Nakagawa, S. Kosai, E. Yamasue, Life cycle resource use of nuclear power generation considering total material requirement, J Clean Prod 363 (2022) 132530.
[12] Caineng Zou, M.A. Feng, P.A.N. Songqi, L.I.N. Minjie, G. Zhang, B. Xiong, et al., Earth energy evolution, human development and carbon neutral strategy, Petrol. Explor. Dev. 49 (2022) 468–488.
[13] L. Liu, H. Guo, L. Dai, M. Liu, Y. Xiao, T. Cong, et al., The role of nuclear energy in the carbon neutrality goal, Prog. Nucl. Energy 162 (2023) 104772.
[14] R. Chen, G.H. Su, K. Zhang, Analysis on the high-quality development of nuclear energy under the goal of peaking carbon emissions and achieving carbon neutrality, Carbon Neutrality 1 (2022) 33.
[15] R. Zhu, C. Zhang, L. Zhu, L. Liu, F. Huo, Y. Wang, et al., "Three-dimensional environment-friendly" amino acid functionalized chitosan: uranium adsorption performance and mechanism research, Carbohydr. Polym. 343 (2024) 122464, https://doi.org/10.1016/j.carbpol.2024.122464.
[16] L. Yang, X. Luo, L. Yan, Y. Zhou, S. Yu, H. Ju, et al., Efficient selective adsorption of uranium using a novel eco-friendly chitosan-grafted adenosine 5′-monophosphate foam, Carbohydr. Polym. 285 (2022) 119157.

[17] Q. Xin, Q. Wang, K. Luo, Z. Lei, E. Hu, H. Wang, et al., Mechanism for the seleikctive adsorption of uranium from seawater using carboxymethyl-enhanced polysaccharide-based amidoxime adsorbent, Carbohydr. Polym. 324 (2024) 121576.
[18] Y.-A. Boussouga, J. Joseph, H. Stryhanyuk, H.H. Richnow, A.I. Schäfer, Adsorption of uranium (VI) complexes with polymer-based spherical activated carbon, Water Res 249 (2024) 120825.
[19] L. Zhu, C. Zhang, F. Ma, C. Bi, R. Zhu, C. Wang, et al., Hierarchical self-assembled polyimide microspheres functionalized with amidoxime groups for uranium-containing wastewater remediation, ACS Appl. Mater. Interfaces 15 (2023) 5577–5589.
[20] C. Bi, C. Zhang, W. Xu, F. Ma, L. Zhu, R. Zhu, et al., Highly efficient antibacterial adsorbent for recovering uranium from seawater based on molecular structure design of PCN-222 post-engineering, Desalination 545 (2023) 116169.
[21] D. Mei, L. Liu, B. Yan, Adsorption of uranium (VI) by metal-organic frameworks and covalent-organic frameworks from water, Coord. Chem. Rev. 475 (2023) 214917.
[22] E.C. Emenike, S.S. Emmanuel, K.O. Iwuozor, K.C. Okwu, A.G. Adeniyi, 12 - Plant biomass materials in petrochemical application, in: M. Jawaid, A. Khan, Asiri Ahmed, AMBT-PBA (Eds.), Acad. Press, Academic Press, 2024, pp. 351–383, https://doi.org/10.1016/B978-0-443-15465-2.00015-X.
[23] A.A. Bayode, S.S. Emmanuel, K.D. Terlanga, Chapter 19 - nanomaterials and their derivative biocomposites for dye adsorption, in: A.H. Jagaba, S.R. Mohamed Kutty, M.H. Isa, Birniwa AHBT-EB for DA (Eds.), Eng. Biocomposites Dye Adsorpt, Elsevier, 2025, pp. 313–337, https://doi.org/10.1016/B978-0-443-29877-6.00019-6.
[24] A.A. Bayode, S. Sunday Emmanuel, S.O. Sanni, F. Lakhdar, L. Fu, J. Shang, et al., Biogenic fabrication of spinel nickel ferrite imprinted on bifurcaria bifurcata macro-alga activated carbon for the adsorption of ciprofloxacin and metronidazole, Chem. Eng. Sci. 302 (2025) 120843, https://doi.org/10.1016/j.ces.2024.120843.
[25] A.A. Bayode, C. Olisah, S.S. Emmanuel, M.O. Adesina, D.T. Koko, Sequestration of steroidal estrogen in aqueous samples using an adsorption mechanism: a systemic scientometric review, RSC Adv. 13 (2023) 22675–22697.
[26] C.T. Umeh, A.B. Akinyele, N.H. Okoye, S.S. Emmanuel, K.O. Iwuozor, I.P. Oyekunle, et al., Recent approach in the application of nanoadsorbents for malachite green (MG) dye uptake from contaminated water: a critical review, Environ. Nanotechnol. Monit. Manag. 20 (2023) 100891, https://doi.org/10.1016/j.enmm.2023.100891.
[27] J.O. Ighalo, B. Yao, Y. Zhou, K.O. Iwuozor, I. Anastopoulos, C.O. Aniagor, et al., Chapter15 - utilization of avocado (Persea americana) adsorbents for the elimination of pollutants from water: a review, in: I. Anastopoulos, E. Lima, L. Meili, Giannakoudakis DBT-B-DM for EA (Eds.), Biomass-Derived Mater. Environ. Appl., Elsevier, 2022, pp. 333–348, https://doi.org/10.1016/B978-0-323-91914-2.00016-7.
[28] T. Sharma, I.G. Hakeem, A.B. Gupta, J. Joshi, K. Shah, A.K. Vuppaladadiyam, et al., Parametric influence of process conditions on thermochemical techniques for biochar production: a state-of-the-art review, J. Energy Inst. (2024) 101559.
[29] Í.V. do Nascimento, L.G. Fregolente, Araújo Pereira AP. de, C.D. V. do Nascimento, J.C.A. Mota, O.P. Ferreira, et al., Biochar as a carbonaceous material to enhance soil quality in drylands ecosystems: a review, Environ. Res. 233 (2023) 116489.
[30] A. Saravanan, P.S. Kumar, Biochar derived carbonaceous material for various environmental applications: systematic review, Environ. Res. 214 (2022) 113857.
[31] T.L. Adewoye, S. Stephen Emmanuel, E. Ebuka Chizitere, O.I. Kingsley, B. Emmanuel, Umar H. Hambali, et al., Dual-phase valorization of chicken feathers and Delonix regia biomass into biochar and pozzolan using a top-lit updraft gasifier, Biofuels (2025) 1–13, https://doi.org/10.1080/17597269.2025.2504845.
[32] K.O. Iwuozor, S.E. Sunday, A.O. Ezzat, E.C. Emenike, O.H. Abd-Elkader, H.A. Al-Lohedan, et al., Repurposing spent sugarcane bagasse biosorbent from waste lubricating oil spill into biochar, Sugar. Tech. 27 (2025) 1290–1299, https://doi.org/10.1007/s12355-025-01579-1.
[33] J.O. Ighalo, J. Conradie, C.R. Ohoro, J.F. Amaku, K.O. Oyedotun, N. W. Maxakato, et al., Biochar from coconut residues: an overview of production, properties, and applications, Ind. Crops. Prod. 204 (2023) 117300.
[34] S. Dou, X.-X. Ke, Z.-D. Shao, L.-B. Zhong, Q.-B. Zhao, Y.-M. Zheng, Fish scale-based biochar with defined pore size and ultrahigh specific surface area for highly efficient adsorption of ciprofloxacin, Chemosphere 287 (2022) 131962.
[35] D. Ma, Y. Yang, B. Liu, G. Xie, C. Chen, N. Ren, et al., Zero-valent iron and biochar composite with high specific surface area via K2FeO4 fabrication enhances sulfadiazine removal by persulfate activation, Chem. Eng. J. 408 (2021) 127992.
[36] J. Qu, S. Wang, L. Jin, Y. Liu, R. Yin, Z. Jiang, et al., Magnetic porous biochar with high specific surface area derived from microwave-assisted hydrothermal and pyrolysis treatments of water hyacinth for Cr (VI) and tetracycline adsorption from water, Bioresour. Technol. 340 (2021) 125692.
[37] K.O. Iwuozor, E. Chizitere Emenike, J.O. Ighalo, F.O. Omoarukhe, P.E. Omuku, A. George Adeniyi, A review on the thermochemical conversion of sugarcane bagasse into biochar, Clean Mater. 6 (2022) 100162, https://doi.org/10.1016/j.clema.2022.100162.
[38] W. Wang, R. Kang, Y. Yin, S. Tu, L. Ye, Two-step pyrolysis biochar derived from agro-waste for antibiotics removal: mechanisms and stability, Chemosphere 292 (2022) 133454, https://doi.org/10.1016/j.chemosphere.2021.133454.
[39] D.L.T. Nguyen, Q.A. Binh, X.C. Nguyen, T.T. Huyen Nguyen, Q.N. Vo, T.D. Nguyen, et al., Metal salt-modified biochars derived from agro-waste for effective Congo red dye removal, Environ Res 200 (2021) 111492, https://doi.org/10.1016/j.envres.2021.111492.
[40] O. Gotore, T.P. Masere, M.T. Muronda, The immobilization and adsorption mechanisms of agro-waste based biochar: a review on the effectiveness of pyrolytic temperatures on heavy metal removal, Environ. Chem. Ecotoxicol. 6 (2024) 92–103.
[41] S. Maji, D.H. Dwivedi, N. Singh, S. Kishor, M. Gond, Agricultural waste: its impact on environment and management approaches, Emerg Eco-Friendly Green Technol Wastewater Treat (2020) 329–351.
[42] A. Thakur, R. Kumar, P.K. Sahoo, Uranium and Fluoride removal from aqueous solution using biochar: a critical review for understanding the role of feedstock types, mechanisms, and modification methods, Water 14 (2022), https://doi.org/10.3390/w14244063.
[43] M. Sharma, Yadav L. Anshika, P. Sharma, V. Chandra Janu, R. Gupta, Breaking new ground: innovative adsorbents for uranium and thorium ions removal and environmental cleanup, Coord. Chem. Rev. 517 (2024) 216008, https://doi.org/10.1016/j.ccr.2024.216008.
[44] S.A. Fahad, M.S. Nawab, M.A. Shaida, S. Verma, M.U. Khan, V. Siddiqui, et al., Carbon based adsorbents for the removal of U (VI) from aqueous medium: a state of the art review, J. Water Process. Eng. 52 (2023) 103458.
[45] S.S. Emmanuel, A.A. Adesibikan, O.T. Ore, A.A. Bayode, H. Badamasi, S.O. Sanni, et al., A comprehensive review on biomass waste-derived biochar for sustainable adsorptive remediation of hazardous radio-contaminants, Waste Biomass Valorization 16 (2025) 2029–2073.
[46] S.S. Emmanuel, A.A. Adesibikan, C. Olusola Olawoyin, A.A. Bayode, A review of antithrombolytic, anticoagulant, and antiplatelet activities of biosynthesized metallic nanostructured multifunctional materials, ChemistrySelect 8 (2023) e202302712, https://doi.org/10.1002/slct.202302712.
[47] G. Li, J. Yao, A review of in situ leaching (ISL) for uranium mining, Mining 4 (2024) 120–148.
[48] C. Degueldre, M.J. Joyce, Evidence and uncertainty for uranium and thorium abundance: a review, Prog. Nucl. Energy. 124 (2020) 103299, https://doi.org/10.1016/j.pnucene.2020.103299.
[49] J. Mehdipour Ghazi, M. Moazzen, M. Fayek, Petrologic exploration criteria for magmatism-related uranium deposits: a review, Int. Geol. Rev. 66 (2024) 1423–1452.

[50] M. Yin, Y. Zhou, D.C.W. Tsang, J. Beiyuan, L. Song, J. She, et al., Emergent thallium exposure from uranium mill tailings, J. Hazard. Mater. 407 (2021) 124402.
[51] S. Akash, B. Sivaprakash, V.C.V. Raja, N. Rajamohan, G. Muthusamy, Remediation techniques for uranium removal from polluted environment—Review on methods, mechanism and toxicology, Environ. Pollut. 302 (2022) 119068.
[52] D.J. Lapworth, B. Brauns, S. Chattopadhyay, D.C. Gooddy, S.E. Loveless, A.M. MacDonald, et al., Elevated uranium in drinking water sources in basement aquifers of southern India, Appl. Geochem. 133 (2021) 105092.
[53] S.K. Sahoo, V.N. Jha, A.C. Patra, S.K. Jha, M.S. Kulkarni, Scientific background and methodology adopted on derivation of regulatory limit for uranium in drinking water—a global perspective, Environ. Adv. 2 (2020) 100020.
[54] H. Yasuda, H. Fumoto, T. Saito, S. Sugawara, S. Tsuchida, Consideration on the intergenerational ethics on uranium waste disposal, Curr. Environ. Health Rep. 11 (2024) 318–328.
[55] H. Feely, The impact of geological dating upon the interpretation of biblical chronology, Creat. Evol. Early Am. Sci. Affil. (2021) 376–379. Routledge.
[56] S.H. Haneklaus, H. Windmann, M. Maekawa, L. Zhang, E. Schnug, Diet controls uranium intake and aggravates health hazards, Med. Res. Arch. 9 (2021).
[57] M. van Gerwen, N. Alpert, W. Lieberman-Cribbin, P. Cooke, K. Ziadkhanpour, B. Liu, et al., Association between uranium exposure and thyroid health: a National Health and Nutrition Examination Survey analysis and ecological study, Int. J. Environ. Res. Publ. Health 17 (2020) 712.
[58] B. Vellingiri, A deeper understanding about the role of uranium toxicity in neurodegeneration, Environ. Res. 233 (2023) 116430.
[59] Y. Yang, C. Dai, X. Chen, B. Zhang, X. Li, W. Yang, et al., Role of uranium toxicity and uranium-induced oxidative stress in advancing kidney injury and endothelial inflammation in rats, BMC Pharmacol. Toxicol. 25 (2024) 14.
[60] Y. Guéguen, M. Frerejacques, Review of knowledge of uranium-induced kidney toxicity for the development of an adverse outcome pathway to renal impairment, Int. J. Mol. Sci. 23 (2022) 4397.
[61] A.M. Horvit, D.A. Molony, A systematic review and meta-analysis of mortality and kidney function in uranium-exposed individuals, Environ. Res. (2024) 118224.
[62] M. Ma, R. Wang, L. Xu, M. Xu, S. Liu, Emerging health risks and underlying toxicological mechanisms of uranium contamination: lessons from the past two decades, Environ. Int. 145 (2020) 106107, https://doi.org/10.1016/j.envint.2020.106107.
[63] L.A. Mohamed, C.O. Aniagor, A.A. Aly, A. Hashem, Removal of chromium (VI) and acid orange 142 dye from contaminated wastewater using bio-waste mycelium of Aspergillus ustus: extraction, isotherms and kinetics studies, Water Conserv Sci Eng 8 (2023) 31.
[64] J.O. Ighalo, V.E. Ojukwu, C.T. Umeh, C.O. Aniagor, C.E. Chinyelu, O.J. Ajala, et al., Recent advances in the adsorptive removal of 2,4-dichlorophenoxyacetic acid from water, J. Water Process. Eng. 56 (2023) 104514, https://doi.org/10.1016/j.jwpe.2023.104514.
[65] A.D. Wiersum, J.-S. Chang, C. Serre, P.L. Llewellyn, An adsorbent performance indicator as a first step evaluation of novel sorbents for gas separations: application to metal–organic frameworks, Langmuir 29 (2013) 3301–3309.
[66] S. Ahmadi, S. Ghosh, A. Malloum, M. Sillanpää, C.A. Igwegbe, P. E. Ovuoraye, et al., Amoxicillin adsorption from aqueous solution by magnetite iron nanoparticles: molecular modelling and simulation, Indian Chem. Eng. 66 (2024) 1–14.
[67] K.O. Iwuozor, C.T. Umeh, S.S. Emmanuel, E.C. Emenike, A.U. Egbemhenghe, O.T. Ore, et al., A comprehensive review on the sequestration of dyes from aqueous media using maize-/corn-based adsorbents, Water Pract. Technol. 18 (2023) 3065–3108.
[68] J. Jin, S. Li, X. Peng, W. Liu, C. Zhang, Y. Yang, et al., HNO3 modified biochars for uranium (VI) removal from aqueous solution, Bioresour. Technol. 256 (2018) 247–253.
[69] X. Wang, J. Feng, Y. Cai, M. Fang, M. Kong, A. Alsaedi, et al., Porous biochar modified with polyethyleneimine (PEI) for effective enrichment of U(VI) in aqueous solution, Sci. Total Environ 708 (2020) 134575, https://doi.org/10.1016/j.scitotenv.2019.134575.
[70] H. Li, X. Zhang, C. Luo, H. Wang, Z. Zou, L. Liu, et al., Pomelo peel derived phosphorus-doped biochar for efficient disposal of uranium-containing nuclear wastewater: experimental and theoretical perspectives, Sep. Purif. Technol. 333 (2024) 125947, https://doi.org/10.1016/j.seppur.2023.125947.
[71] W. Ahmed, S. Mehmood, M. Qaswar, S. Ali, Z.H. Khan, H. Ying, et al., Oxidized biochar obtained from rice straw as adsorbent to remove uranium (VI) from aqueous solutions, J. Environ. Chem. Eng. 9 (2021) 105104.
[72] J. Lv, H. Xia, Q. Ren, Y. Wang, Y. Liu, Z. Feng, et al., Hydrothermal fabrication of amino functionalized lotus seedpods-derived biochar for efficient removal of uranium (VI), J. Radioanal. Nucl. Chem. 332 (2023) 4075–4087.
[73] J. Liao, T. Xiong, Z. Zhao, L. Ding, W. Zhu, Y. Zhang, Synthesis of a novel environmental-friendly biocarbon composite and its highly efficient removal of uranium(VI) and thorium(IV) from aqueous solution, J. Clean. Prod. 374 (2022) 134059, https://doi.org/10.1016/j.jclepro.2022.134059.
[74] J. Liao, X. He, Y. Zhang, W. Zhu, L. Zhang, Z. He, Bismuth impregnated biochar for efficient uranium removal from solution: adsorption behavior and interfacial mechanism, Sci. Total Environ. 819 (2022) 153145, https://doi.org/10.1016/j.scitotenv.2022.153145.
[75] J. Liao, L. Ding, Y. Zhang, W. Zhu, Efficient removal of uranium from wastewater using pig manure biochar: understanding adsorption and binding mechanisms, J. Hazard. Mater. 423 (2022) 127190, https://doi.org/10.1016/j.jhazmat.2021.127190.
[76] K. Narasimharao, G.K.R. Angaru, Z.H. Momin, S. Al-Thabaiti, M. Mokhtar, A. Alsheshri, et al., Orange waste Biochar-Magnesium Silicate (OBMS) composite for enhanced removal of U(VI) ions from aqueous solutions, J. Water Process. Eng. 51 (2023) 103359, https://doi.org/10.1016/j.jwpe.2022.103359.
[77] D. Ying, P. Hong, F. Jiali, T. Qinqin, L. Yuhui, W. Youqun, et al., Removal of uranium using MnO2/orange peel biochar composite prepared by activation and in-situ deposit in a single step, Biomass Bioenergy 142 (2020) 105772.
[78] F. Liu, S. Wang, C. Zhao, B. Hu, Constructing coconut shell biochar/MXenes composites through self-assembly strategy to enhance U (VI) and Cs (I) immobilization capability, Biochar. 5 (2023) 31.
[79] Q. Zhao, Z. Xu, Z. Yu, Straw-derived biochar as the potential adsorbent for U (VI) and Th (IV) removal in aqueous solutions, Biomass Convers. Biorefinery 13 (2023) 15707–15718.
[80] K. Philippou, I. Anastopoulos, C. Dosche, I. Pashalidis, Synthesis and characterization of a novel Fe3O4-loaded oxidized biochar from pine needles and its application for uranium removal. Kinetic, thermodynamic, and mechanistic analysis, J. Environ. Manag. 252 (2019) 109677.
[81] Y. Wang, X. Wu, X. Liu, C. Cai, C. Liang, L. Dai, et al., Microbial etch: a novel construction method of functionalized biochar for enhanced uranium extraction in radioactive wastewater, Chemosphere 361 (2024) 142544, https://doi.org/10.1016/j.chemosphere.2024.142544.
[82] Y. Zhang, X. Liu, K. Jiang, J. Feng, Y. Liu, Efficient adsorption of U (VI) using potassium permanganate-modified biochar: adsorption behavior and mechanism, J. Radioanal. Nucl. Chem. (2025) 1–11.
[83] S.N. Guilhen, O. Mašek, N. Ortiz, J.C. Izidoro, D.A. Fungaro, Pyrolytic temperature evaluation of macauba biochar for uranium adsorption from aqueous solutions, Biomass Bioenergy 122 (2019) 381–390, https://doi.org/10.1016/j.biombioe.2019.01.008.
[84] S. Neusatz Guilhen, S. Rovani, L. Pitol Filho, D. Alves Fungaro, Kinetic study of uranium removal from aqueous solutions by macaúba biochar, Chem. Eng. Commun. 206 (2019) 1354–1366.
[85] T. Ye, B. Huang, Y. Wang, L. Zhou, Z. Liu, Rapid removal of uranium (VI) using functionalized luffa rattan biochar from

aqueous solution, Colloids Surfaces A Physicochem Eng Asp 606 (2020) 125480.
[86] X. He, C. Zhou, Y. Xu, P. Yang, Preparation of alkali-activated nitrogen-doped durian shell biochar and efficient removal of uranyl ions, J. Radioanal. Nucl. Chem. (2025) 1−14.
[87] L.P. Lingamdinne, J.-S. Choi, G.K.R. Angaru, R.R. Karri, J.-K. Yang, Y.-Y. Chang, et al., Magnetic-watermelon rinds biochar for uranium-contaminated water treatment using an electromagnetic semi-batch column with removal mechanistic investigations, Chemosphere 286 (2022) 131776.
[88] D. Xia, Y. Liu, X. Cheng, P. Gu, Q. Chen, Z. Zhang, Temperature-tuned fish-scale biochar with two-dimensional homogeneous porous structure: a promising uranium extractant, Appl. Surf. Sci. 591 (2022) 153136, https://doi.org/10.1016/j.apsusc.2022.153136.
[89] T. Zeng, Y. Fu, M. Yang, Q. Deng, S. Chen, Y. Liu, et al., U(VI) removal by zerovalent manganese modified corn straw biochar in acidic wastewater: efficiency, characteristics and mechanism, Chemosphere 373 (2025) 144163, https://doi.org/10.1016/j.chemosphere.2025.144163.
[90] Y. Zhu, M. Shaban, N.S. Alharbi, X. Ren, C. Chen, Insight into the enhanced removal of U(VI) with Fe−Ni bimetallic particles loaded on biochar, Langmuir 41 (2025) 2880−2891, https://doi.org/10.1021/acs.langmuir.4c04766.
[91] L. Dai, L. Li, W. Zhu, H. Ma, H. Huang, Q. Lu, et al., Post-engineering of biochar via thermal air treatment for highly efficient promotion of uranium(VI) adsorption, Bioresour. Technol. 298 (2020) 122576, https://doi.org/10.1016/j.biortech.2019.122576.
[92] Y. Sun, N. Yuan, Y. Ge, T. Ye, Z. Yang, L. Zou, et al., Adsorption behavior and mechanism of U(VI) onto phytic Acid-modified Biochar/MoS2 heterojunction materials, Sep. Purif. Technol. 294 (2022) 121158, https://doi.org/10.1016/j.seppur.2022.121158.
[93] C. Li, P. Mao, G. Feng, C. Cai, Efficient adsorption properties of uranium from wastewater using biochar derived from Hami-melon peels, J Radioanal. Nucl. Chem. (2025) 1−13.
[94] X. Li, H. Pan, M. Yu, M. Wakeel, J. Luo, N.S. Alharbi, et al., Macroscopic and molecular investigations of immobilization mechanism of uranium on biochar: EXAFS spectroscopy and static batch, J. Mol. Liq. 269 (2018) 64−71.
[95] M. Albayari, M.K. Nazal, F.I. Khalili, N. Nordin, R. Adnan, Biochar derived from Salvadora persica branches biomass as low-cost adsorbent for removal of uranium (VI) and thorium (IV) from water, J. Radioanal. Nucl. Chem. 328 (2021) 669−678.
[96] J. Li, M. Zhang, Q. Kong, T. Zeng, Y. Mao, J. Liu, et al., Effects and mechanism of uranium(VI) removal by wood biochar loaded with MnFe2O4, J Taiwan Inst Chem Eng 166 (2025) 105532, https://doi.org/10.1016/j.jtice.2024.105532.
[97] Z. Zhang, X. Cao, P. Liang, Y. Liu, Adsorption of uranium from aqueous solution using biochar produced by hydrothermal carbonization, J Radioanal. Nucl. Chem. 295 (2013) 1201−1208.
[98] M. Li, H. Liu, T. Chen, C. Dong, Y. Sun, Synthesis of magnetic biochar composites for enhanced uranium(VI) adsorption, Sci. Total Environ. 651 (2019) 1020−1028, https://doi.org/10.1016/j.scitotenv.2018.09.259.
[99] Y. Liu, Y. Wang, H. Xia, Q. Wang, X. Chen, J. Lv, et al., Low-cost reed straw-derived biochar prepared by hydrothermal carbonization for the removal of uranium (VI) from aqueous solution, J. Radioanal. Nucl. Chem. 331 (2022) 3915−3925.
[100] Z. Xia, C.-R. Zhang, X.-J. Chen, Y.-J. Cai, S.-M. Yi, R.-P. Liang, et al., Phosphorylated litchi shell-derived biochar for removal U(VI) from mining wastewater, Chem. Eng. Sci. 301 (2025) 120708, https://doi.org/10.1016/j.ces.2024.120708.
[101] W. Ahmed, S. Mehmood, A. Núñez-Delgado, S. Ali, M. Qaswar, Z. H. Khan, et al., Utilization of Citrullus lanatus L. seeds to synthesize a novel MnFe2O4-biochar adsorbent for the removal of U (VI) from wastewater: insights and comparison between modified and raw biochar, Sci. Total Environ. 771 (2021) 144955.
[102] E. Zhao, A. Wang, L. Huang, C. Chen, M. Qiu, Mechanism and chemical stability of U (VI) removal by magnetic Fe3O4@ biochar composites, Nat. Environ. Pollut. Technol. 21 (2022) 263−268.
[103] C.O. Aniagor, C.A. Igwegbe, J.O. Ighalo, S.N. Oba, Adsorption of doxycycline from aqueous media: a review, J. Mol. Liq. 334 (2021) 116124, https://doi.org/10.1016/j.molliq.2021.116124.
[104] A.A. Adesibikan, S.S. Emmanuel, S.A. Nafiu, M.J. Tachia, K.O. Iwuozor, E.C. Emenike, et al., A review on sustainable photocatalytic degradation of agro-organochlorine and organophosphorus water pollutants using biogenic iron and iron oxide-based nanoarchitecture materials, Desalination Water Treat. 320 (2024) 100591, https://doi.org/10.1016/j.dwt.2024.100591.
[105] S.S. Emmanuel, A.A. Adesibikan, O.D. Saliu, Phytogenically bioengineered metal nanoarchitecture for degradation of refractory dye water pollutants: a pragmatic minireview, Appl. Organomet. Chem. 37 (2023) e6946.
[106] M.M. Majd, V. Kordzadeh-Kermani, V. Ghalandari, A. Askari, M. Sillanpää, Adsorption isotherm models: a comprehensive and systematic review (2010− 2020), Sci. Total Environ. 812 (2022) 151334.
[107] C.A. Igwegbe, J.O. Ighalo, S. Ghosh, S. Ahmadi, V.I. Ugonabo, Pistachio (Pistacia vera) waste as adsorbent for wastewater treatment: a review, Biomass Convers. Biorefinery 13 (2023) 8793−8811.
[108] S. Alvarez-García, J.J. Ramírez-García, F. Granados-Correa, J.C. Sánchez-Meza, Determination of kinetic, isotherm, and thermodynamic parameters of the methamidophos adsorption onto cationic surfactant-modified zeolitic materials, Water Air Soil Pollut. 229 (2018) 1−17.
[109] E.C. Lima, A.A. Gomes, H.N. Tran, Comparison of the nonlinear and linear forms of the van't Hoff equation for calculation of adsorption thermodynamic parameters (Δ S° andΔ H°), J. Mol. Liq. 311 (2020) 113315.
[110] H.N. Tran, E.C. Lima, R.-S. Juang, J.-C. Bollinger, H.-P. Chao, Thermodynamic parameters of liquid−phase adsorption process calculated from different equilibrium constants related to adsorption isotherms: a comparison study, J. Environ. Chem. Eng. 9 (2021) 106674.
[111] M.N. Sahmoune, Evaluation of thermodynamic parameters for adsorption of heavy metals by green adsorbents, Environ. Chem. Lett. 17 (2019) 697−704.
[112] E.C. Lima, A. Hosseini-Bandegharaei, J.C. Moreno-Piraján, I. Anastopoulos, A critical review of the estimation of the thermodynamic parameters on adsorption equilibria. Wrong use of equilibrium constant in the Van't Hoof equation for calculation of thermodynamic parameters of adsorption, J. Mol. Liq. 273 (2019) 425−434.
[113] S.S. Emmanuel, A.A. Adesibikan, Harvesting surface (interfacial) energy for tribocatalytic degradation of hazardous dye pollutants using nanostructured materials: a review, J. Chinese Chem. Soc. 71 (2024) 944−977, https://doi.org/10.1002/jccs.202400157.
[114] H. Badamasi, S.O. Sanni, O.T. Ore, A.A. Bayode, D.T. Koko, O.K. Akeremale, et al., Eggshell waste materials-supported metal oxide nanocomposites for the efficient photocatalytic degradation of organic dyes in water and wastewater: a review, Bioresour. Technol. Rep. 26 (2024) 101865, https://doi.org/10.1016/j.biteb.2024.101865.
[115] S.S. Emmanuel, A.A. Adesibikan, C.O. Olawoyin, M.O. Idris, Photocatalytic degradation of maxilon dye pollutants using nano-architecture functional materials: a review, ChemistrySelect 9 (2024) e202400316, https://doi.org/10.1002/slct.202400316.
[116] A.A. Adesibikan, S.S. Emmanuel, C.O. Olawoyin, P. Ndungu, Cellulosic metallic nanocomposites for photocatalytic degradation of persistent dye pollutants in aquatic bodies: a pragmatic review, J. Organomet. Chem. (2024) 123087, https://doi.org/10.1016/j.jorganchem.2024.123087.
[117] S. Sutar, P. Patil, J. Jadhav, Recent advances in biochar technology for textile dyes wastewater remediation: a review, Environ. Res. 209 (2022) 112841, https://doi.org/10.1016/j.envres.2022.112841.